Trumbull, R. B., Slack, J. F., Krienitz, M.-S., Belkin, H. E., Wiedenbeck, M. (2011): Fluid sources and metallogenesis in the Blackbird Co-Cu-Au-Bi-Y-REE district, Idaho, USA: constraints from chemical and boron isotope variations in tourmaline. - Canadian Mineralogist, 49, 1, 225-244

DOI: 10.3749/canmin.49.1.225

FLUID SOURCES AND METALLOGENESIS IN THE BLACKBIRD Co-Cu-Au-Bi-Y-REE DISTRICT, IDAHO, U.S.A.: INSIGHTS FROM MAJOR-ELEMENT AND BORON ISOTOPIC COMPOSITIONS OF TOURMALINE

Robert B. Trumbull*
GFZ German Research Centre for Geosciences, Telegrafenberg, 14473 Potsdam, Germany

John F. Slack
U.S. Geological Survey, National Center, Mail Stop 954, Reston Virginia 20192, U.S.A.

Marc-Sebastian Krienitz
GFZ German Research Centre for Geosciences, Telegrafenberg, 14473 Potsdam, Germany

Harvey E. Belkin
U.S. Geological Survey, National Center, Mail Stop 956, Reston Virginia 20192, U.S.A.

Michael Wiedenbeck
GFZ German Research Centre for Geosciences, Telegrafenberg, 14473 Potsdam, Germany

*Corresponding author: E-mail: robert.trumbull@gfz-potsdam.de
Telephone: +49-331-2881495; Fax: +49-331-2881474

ABSTRACT

Tourmaline is a widespread mineral in the Mesoproterozoic Blackbird Co-Cu-Au-Bi-Y-REE district, Idaho, where it occurs in both mineralized zones and wallrocks. We report here major-element and B-isotope compositions of tourmaline from stratabound sulfide deposits and their metasedimentary wallrocks, from mineralized and barren tourmaline breccia pipes, from late barren quartz veins, and from Mesoproterozoic granite. Tourmalines are aluminous, intermediate schorl-dravite with Fe/(Fe+Mg) ratios of 0.30 to 0.85 and 10 % to 50 % X-site vacancies. Compositional zoning is prominent only in tourmaline from breccias and quartz-veins; crystal rims are enriched in Mg, Ca and Ti, and depleted in Fe and Al relative to cores. The chemical composition of tourmaline does not correlate with the presence or absence of mineralization.

The $\delta^{11}B$ values fall into two groups. Isotopically light tourmaline (-21.7 to -7.6 ‰) occurs in unmineralized samples from wallrocks, late quartz veins and Mesoproterozoic granite, whereas heavy tourmaline (-6.9 to +3.2 ‰) is spatially associated with mineralization (stratabound and breccia-hosted), and is also found in barren breccia. At an inferred temperature of 300°C, boron in the hydrothermal fluid associated with mineralization had $\delta^{11}B$ values of -3 to +7 ‰. The high end of this range indicates a marine source of the boron. A likely scenario involves leaching of boron principally from marine carbonate beds or B-bearing evaporites in Mesoproterozoic strata of the region.The $\delta^{11}B$ values of the isotopically light tourmaline in the sulfide deposits are attributed to recrystallization during Cretaceous metamorphism, superimposed on a light boron component derived from footwall siliciclastic sediments (*e.g.*, marine clays) during Mesoproterozoic mineralization, and possibly a minor component of light boron from a magmatic-hydrothermal fluid. The metal association of Bi-Be-Y-REE in the Blackbird ores suggests some magmatic input, but involvement of granite-derived fluids cannot be conclusively established from the present database.

Key words: *Blackbird, Idaho, cobalt belt, stratabound sulfides, tourmaline, chemical composition, boron isotopes, SIMS, fluid sources, metallogeny*

INTRODUCTION

The wide stability range of tourmaline, and its compositional variability and resistance to alteration, make this mineral a useful geochemical tracer (*e.g.*, Henry & Guidotti 1985, Slack 1996, Bebout & Nakamura 2003). Tourmaline can be particularly valuable in studies of hydrothermal mineral deposits because it is the main host for boron in most rocks, and because the boron isotopic composition is sensitive to changes in fluid source, P-T conditions of crystallization, and phase changes such as boiling or fluid unmixing (Palmer & Slack 1989, Slack *et al.* 1993, Palmer & Swihart 1996, Smith & Yardley 1996, Trumbull & Chaussidon, 1999, Taylor *et al.* 1999, Jiang *et al.* 1999, 2002, Kasemann *et al.* 2000, Mlynarczyk & Williams-Jones 2006, Krienitz *et al.* 2008, Marschall *et al.* 2008, Xavier *et al.* 2008, Trumbull *et al.* 2008, 2009, Garda *et al.* 2009, Pal *et al.* 2010).

In this contribution, we present the first study of chemical and boron isotope compositions of tourmaline from the Blackbird district in central Idaho, U.S.A., with the aim of gaining insight into the source of the contained boron and mineralizing fluids. The Blackbird district is metallogenically important because it hosts the largest known reserves of cobalt in the United States. Stratabound sulfide deposits of this district, occurring within the central part of the ~60-km-long Idaho cobalt belt (ICB), have been interpreted for over two decades as products of syngenetic to diagenetic mineralization (*e.g.*, Modreski 1985, Eiseman 1988, Nash & Hahn 1989, Nold 1990, Evans *et al.* 1995, Bending & Scales 2001). Recent work has identified several diagnostic mineralogical and geochemical features in the deposits, including locally high contents of Bi, Y, rare earth elements (REE), and Be, which together suggest mineralization in a magmatic-related, iron oxide-copper-gold (IOCG) system (Slack 2011). Our study seeks additional constraints on the origin of these enigmatic deposits by using tourmaline as a geochemical tracer of boron sources and its evolution in the district.

GEOLOGICAL SETTING

Sulfide deposits of the Blackbird district occur mainly within interlayered siltite, argillite, and quartzite of the Mesoproterozoic Apple Creek Formation (Fig. 1). The maximum age of this stratigraphic unit, previously mapped as the lithologically similar Yellowjacket Formation, is 1409 ± 10 Ma based on Sensitive High-Resolution Ion Microprobe (SHRIMP) U-Pb dating of detrital zircons

(Aleinikoff *et al.* 2011). This unit is intruded on the north side of the district by a large sill-like body of megacrystic granite, which has a SHRIMP U-Pb zircon age of 1377 ± 4 Ma (Aleinikoff *et al.* 2011). Areally smaller, coeval intrusions of coarse metadiabase in this area have a U-Pb zircon age of 1378.7 ± 1.2 Ma (Doughty & Chamberlain 1996). During the Neoproterozoic and Late Cambrian, felsic and minor mafic alkalic plutons were emplaced in the region, the nearest occurring ca. 5 km east of the district (Tysdal *et al.* 2003, Lund *et al.* 2010). Igneous activity resumed during intrusion of the Laramide (~93-54 Ma) Idaho batholith, ca. 30 km northwest of the district, and during intrusion of the Eocene (49-44 Ma) Big Horn Crags pluton ca. 10 km west of the district (see Tysdal *et al.* 2003, Lund & Tysdal 2007).

The oldest deformation in the region is Mesoproterozoic based on the presence of folds in the Yellowjacket Formation that are cut by the 1.37 Ga megacrystic granite (Evans 1986; A.A. Bookstrom, written commun., 2010). Several regional metamorphic events occurred in northern Idaho from ~1463 Ma to ~1064 Ma (Doughty & Chamberlain 2008, Zirakparvar *et al.* 2010), but their effects on rocks of the Blackbird district, if any, are unknown. During the Cretaceous, folding, thrust faulting, and greenschist- to amphibolite-facies metamorphism overprinted rocks and ores in the district (Lund & Tydsal 2007), and led to widespread recrystallization of ore and gangue minerals (Slack 2011, Aleinikoff *et al.* 2011). Cretaceous metamorphism in the study area is recorded by Lu-Hf ages of 151 ± 32 Ma and 112.8 ± 7.7 Ma on garnet (Zirakparvar *et al.* 2007), by an Ar-Ar cooling age of 83 Ma on cleavage-hosted white mica (Lund *et al.* 2007), and by SHRIMP U-Pb ages of 145, 110, and 92 Ma on monazite in the sulfide deposits (Aleinikoff *et al.* 2011).

Types of mineral deposits

The Blackbird district contains three principal types of mineral deposits: (1) stratabound and locally discordant sulfide lenses, (2) discordant tourmaline breccias, and (3) stratabound magnetite-sulfide lenses. The first of these, the stratabound sulfide deposits, is the most important economically, having supplied the majority of cobalt production (Nash & Hahn 1989, Bending & Scales 2001, Bookstrom *et al.* 2007). These deposits vary in thickness from <1 m to 4 m, and show a variety of deformational features including shears, folds, boudins, cusps, and remobilized veins. Based on

detailed underground mapping, Vhay (1948) determined that the sulfide deposits are mainly localized in preexisting structures such as faults, shear zones, and fold axes. Principal ore minerals are cobaltite and chalcopyrite, which occur in a gangue of quartz and biotite with generally minor chlorite, muscovite, garnet, chloritoid, or tourmaline (Anderson 1947, Modreski 1985, Eiseman 1988, Nash & Hahn 1989). Other ore minerals include pyrite, pyrrhotite, arsenopyrite, glaucodot, safflorite, bismuthinite, native bismuth, Bi-tellurides, and gold. Recent geochemical and mineralogical studies have documented previously unknown high Bi contents (up to 9.2 wt %) and occurrences of sparse uraninite and stannite (Slack 2011). Some of the sulfide deposits, such as Sunshine, Merle, Brown Bear, and Ram (Fig. 1), locally contain minor to abundant allanite, apatite, xenotime, or monazite, which in whole-rock analyses produce total REE+Y oxide contents up to 3.66 wt % (Slack 2006, 2011). SHRIMP U-Pb dating of paragenetically early xenotime from the Merle deposit yields an age of 1370 ± 4 Ma, which is within analytical uncertainty of the 1377 ± 4 Ma age of the megacrystic granite (Aleinkoff *et al.* 2011). The Northfield deposit has local concentrations of gadolinite-(Y) (Slack 2011), a Be-rich silicate containing essential Fe, light rare-earth elements (LREE), and Y [$(LREE,Y)_2Fe^{2+}Be_2O(SiO_4)_2$]. Most of the stratabound sulfide deposits are interlayered with distinctive rocks composed mainly of Fe- and Cl-rich biotite, termed biotitite (Nash & Hahn 1989, Nash & Connor 1993), which likely formed by hydrothermal metasomatism of argillaceous sediments.

The discordant tourmaline breccia zones comprise pipes and breccias up to ca. 50 m in diameter that cross-cut metasedimentary rocks of the Apple Creek Formation or the overlying Gunsight Formation (Modreski 1985, Bookstrom *et al.* 2007). The breccias consist of angular to rounded fragments of siltite or quartzite with a matrix of abundant fine-grained tourmaline and lesser quartz. Some of the breccias are mineralized and contain minor to major amounts of disseminated cobaltite; in addition, the Haynes-Stellite breccia (Fig. 1) has abundant fine-grained xenotime (Slack 2011). All of the tourmaline breccia zones except one, both mineralized and barren, are distal (>1 km) to the stratabound sulfide deposits and occur in the stratigraphically higher unit (Gunsight Formation). The exception is a thin (~0.5-m-thick) tourmaline breccia that occurs within the Idaho stratabound sulfide zone (sample GH-BB-19).

149 The third type of mineral deposit in the region consists of stratabound magnetite-sulfide deposits
150 in the Iron Creek area ca. 25 km southeast of the Blackbird district (Fig. 1). These deposits form
151 magnetite-rich lenses up to 5 m thick within siliciclastic metasedimentary rocks of the Apple Creek
152 Formation. Magnetite occurs as massive concentrations, in sulfide-poor veins, and in stratabound
153 layers containing abundant cobaltiferous pyrite and minor chalcopyrite (Nash 1989). The Iron Creek
154 deposits are not part of the tourmaline study presented here.
155
156 ***Tourmaline occurrences***
157 Tourmaline in the Blackbird district occurs in different settings. Within the stratabound sulfide
158 deposits, it typically forms fine-grained (50-100 μm) subhedral to euhedral crystals intergrown with
159 chlorite or muscovite, with or without associated cobaltite (Fig. 2a). It also occurs as fine or coarse
160 euhedral grains disseminated in silicate wallrocks, typically 0.1 mm in the Sunshine deposit and 1 to 3
161 mm in the Ram deposit (Fig. 2b). Textural relationships suggest a contemporaneous precipitation of
162 tourmaline and sulfides in most cases. Tourmaline also occurs as coarse (1-5 mm) euhedral crystals in
163 late quartz veins that cut metamorphic fabrics in wallrocks to the deposits (Fig. 2c). The coarse vein-
164 hosted crystals of tourmaline contrast with those in the tourmaline breccias, which are generally very
165 fine-grained (10-50 μm), and together with fine-grained quartz and local cobaltite, form the matrix to
166 angular or subrounded fragments of siltite and quartzite (Fig. 2d). Tourmaline in the mineralized
167 breccias also appears to be contemporaneous with cobaltite and other sulfides. A different variety of
168 tourmaline breccia occurs ca. 15 km east of the district (Fig. 1), where fine-grained euhedral
169 tourmaline and quartz make up the matrix for angular fragments of brecciated quartzite. Tourmaline
170 also is present as 1- to 3-mm-thick laminae in scapolite-bearing metaevaporite schists of the
171 Yellowjacket Formation (Tysdal & Desborough 1997, Tysdal *et al.* 2003), but this tourmaline was
172 unavailable for our study.
173 The 1377 Ma megacrystic granite contains three types of tourmaline. One occurs within the
174 granite as small (50-100 μm) euhedral grains intergrown with quartz and alkali feldspar, and is
175 interpreted to be magmatic in origin. A second type, also within the granite, forms euhedral grains 50
176 to 100 μm in length interspersed with chlorite and muscovite in pseudomorphs after K-feldspar (Fig.

2e), a texture that suggests a late magmatic to deuteric origin. The third type of tourmaline occurs as coarse 1 to 3 mm euhedral crystals in a planar quartz vein (Fig. 2f), within the granite a few meters from its contact with surrounding metasedimentary rocks, implying a late magmatic-hydrothermal origin for this tourmaline.

Variations in grain size of the tourmaline in most of the non-granitic samples likely reflect metamorphic recrystallization of pre-existing tourmaline. Numerous studies have established that tourmaline recrystallizes during metamorphism, particularly at upper greenschist and higher metamorphic grades and high fluid/rock conditions (*e.g.*, Slack *et al.* 1993, Henry & Dutrow 1996, Sperlich *et al.* 1996, Pesquera *et al.* 2005; Trumbull *et al.* 2009). Disseminated tourmaline in wallrocks to the Ram deposit, for example, ranges from 1 to 3 mm in length and typically is euhedral with well-developed growth-induced zoning (Fig. 2b). These features strongly suggest growth of tourmaline during metamorphism, probably the pervasive Cretaceous metamorphic event in the ICB. In contrast is the very fine-grained (<50 μm) tourmaline that characterizes the tourmaline breccia pipes (Fig. 2d), which is texturally similar to that in the tourmalinized feeder zone of the Sullivan Pb-Zn-Ag deposit in British Columbia and in regional tourmalinite bodies within lower to middle greenschist-facies strata of the Mesoproterozoic Belt and Purcell Supergroups (Slack *et al.* 2000 and references therein). As described in those studies, such very fine-grained tourmaline is likely pre-metamorphic, having formed during primary hydrothermal B metasomatism of argillaceous sediment, whereas coarser tourmaline in the deposits is considered to have formed during metamorphic recrystallization of pre-existing, smaller tourmaline grains. We are uncertain, however, of the extent of metamorphic recrystallization, if any, of the relatively fine-grained tourmaline in several samples, including that in wallrocks to the Sunshine deposit (i.e., sample SS-1A-456, 0.1 mm) and in the mineralized and barren tourmaline breccia pipes (*e.g.*, sample JS-06-32B, up to 0.1 mm).

SAMPLING AND ANALYTICAL METHODS

The tourmaline samples analyzed in this study represent all major types of tourmaline occurrence in the Blackbird district, namely:

(1a) Stratabound sulfide ore zones (GH-BB-20 from the South Idaho deposit, SP-79-803 from the Brown Bear deposit). The relatively fine-grained (mostly <50 μm) tourmaline in the Brown Bear cobaltite-rich sample is considered the best example of primary (unrecrystallized) hydrothermal tourmaline within the ore zones,

(1b) Silicate wallrocks to the stratabound ores (RO5-03-419 from the Ram deposit, SS-1A-456 from the Sunshine deposit; NW-8030-1 from ca. 800 m stratigraphically above the Blackbird deposit, close to the Horseshoe zone),

(2a) Mineralized tourmaline breccias (GH-BB-19 from the Idaho deposit, GH-BB-23 from the Haynes-Stellite deposit, JS-06-32B from the CoNiCu deposit),

(2b) Barren tourmaline breccias (AB-1-Beliel from the Beliel deposit, CoNiCu-tg from the CoNiCu deposit, and BB-DC-4 from the quartzite breccia in the Gunsight Formation east of the district),

(3) Late (probably Cretaceous) planar quartz-tourmaline veins in wallrocks to the sulfide deposits (R97-15-221 from the Ram deposit),

(4a) Quartz-tourmaline vein in the margin of the megacrystic granite (67SB160A),

(4b) Disseminated tourmaline within the megacrystic granite (SA-1-3, SA-1-4).

Electron-microprobe analysis

Chemical analyses of tourmaline were determined on polished thin sections using wavelength-dispersive electron-microprobe analysis (EMPA) at the U.S. Geological Survey in Reston, Virginia. Analyses employed a JEOL JXA-8900/R five-spectometer, fully automated electron microprobe. Samples were examined optically and by back-scatter electron imaging to identify sites for analysis. Analyses were made at 15 kV accelerating voltage and 30 nA beam current as measured with a Faraday cup. Peak and background counting times were 20 and 120 s, respectively, on major and minor elements, and the beam size was approximately 2 μm in diameter. The following natural and synthetic reference materials were used for calibration: Na - synthetic albite, Ti - SPI rutile, Fe - Rockport fayalite, Mg, Si, Ca - Kakanui pyroxene, Al - Lake County plagioclase, K- PSU adularia, Cl - SPI tugtupite, F - synthetic fluorphlogopite, Cr - Bushveld chromite, Mn - synthetic tephroite. The

results were corrected for electron-beam matrix effects, instrumental drift, and deadtime using a Phi–Rho–Z (CITZAF, Armstrong 1995) scheme. Relative trueness of the analytical data, as determined by comparison of measured and published compositions of reference materials, is ~1–2% for oxide concentrations above 1 wt% and ~5–10% for oxide concentrations less than 1 wt%. Detection limits, based on the 3σ deviation of background counts, are as follows: SiO_2 and Cl = 0.02 wt%; TiO_2, Al_2O_3, Cr_2O_3, FeO, MnO, MgO, CaO, and K_2O = 0.03 wt%; Na_2O and F = 0.04 wt%.

Tourmaline structural formulae were calculated from the electron-microprobe data by normalizing to a sum of 15 cations in the tetrahedral and octahedral sites (T+Z+Y) following the approach of Henry & Dutrow (1996). Typical exemplary tourmaline compositions are listed in Table 1; the complete chemical data set is included in the Electronic Supplementary Material (ESM Table 1), available from the Depository of Unpublished Data on the MAC website.

SIMS analysis

Boron isotopic compositions of tourmaline were determined with the CAMECA ims6f SIMS instrument in Potsdam. After electron-microprobe analysis, samples were re-polished with alumina and distilled water, then ultrasonically cleaned with ethanol and sputter coated with a ~35-nm-thick layer of high-purity gold. Where grain size permitted, analyses were made on rim and core portions of each grain. In all but a few cases, SIMS analyses were located directly adjacent to spots previously analysed by EPMA. Boron isotopic analyses employed a nominally 12.5 kV, 0.8 nA $^{16}O^-$ primary beam that was focused to a ~5 µm diameter spot on the sample surface. The use of a liquid nitrogen cold trap provided a secondary ion source pressure in the mid to low 10^{-7} Pa range. Prior to each analysis, a 3-min preburn was used in order to remove the gold coat and establish equilibrium sputtering conditions. The mass spectrometer was operated at a mass resolution power $M/\Delta M \approx 1370$, sufficient to separate the isobaric interference of $^{10}B^1H$ on the ^{11}B mass station. A 150-µm-diameter contrast aperture, an 1800 µm field aperture (equivalent to a 150 µm field of view), and a 50 V energy window were used without any voltage offset. These conditions resulted in a count rate of ~300 kHz for ^{11}B and ~ 80 kHz for ^{10}B on the electron multiplier, to which a 16 ns deadtime correction was

applied. A single analysis consisted of 100 scans of the sequence ^{10}B (2 s) and ^{11}B (1 s), resulting in a total time of about 10 min for each analysis.

Instrumental mass-fractionation (IMF) and analytical quality were monitored by repeated analyses of tourmaline reference materials dravite (HS #108796) and schorl (HS #112566) from the Harvard University Mineralogical Museum and B4 from the Instituto Geocronologia et Geochimica Isotopica, Pisa. Assigned $^{11}B/^{10}B$ ratios of the Harvard tourmalines are reported by Dyar *et al.* (2001), and of B4 by Tonarini *et al.* (2003) and Gonviantini *et al.* (2004). Daily routine was to precede and follow 8-10 analyses of unknowns by 3-5 measurements on the reference tourmalines. This study combines data from 5 SIMS sessions of 2-3 days each, from August, 2008, to August, 2010; data were corrected for IMF factors detemined for each session separately. Results for reference tourmaline analyses during a typical session are given in Table 2. Systematic drift of IMF values occurred in the course of one session, possibly due to fatigue of the electron multiplier, and required correction of the measured isotope ratios from a linear regression of the IMF values (also see Garda *et al.* 2009). The uncertainty of individual analyses (1 sd/mean of 100 blocks) was < 1‰ (1sd) and repeatability of multiple analyses on each reference tourmaline during a session varied from 1-2‰ (n = 5 to 10 typically). The observed variations in average IMF values among the three reference samples are about 2‰, which we take as the best estimate of the total analytical uncertainty. Corrected boron isotope ratios are reported using the $\delta^{11}B$ notation ($\delta^{11}B = \{^{11}B/^{10}B_{Sample}{}^{corr} / {}^{11}B/^{10}B_{RM} - 1\} \times 1000$) relative to the reference material NIST SRM 951, which has a $^{11}B/^{10}B$ ratio of 4.04362 (Cantanzaro *et al.* 1970). Table 3 summarizes the results for all samples from the Blackbird district; the full data set is reported together with corresponding microprobe results in the Electronic Supplementary Material (ESM Table 1), available from the Depository of Unpublished Data on the MAC website.

RESULTS

Tourmaline classification and major-element variations

Tourmaline from all lithologies in the Blackbird district belongs to the alkali group in the nomenclature of Hawthorne & Henry (1999), except for some grains from the quartzite breccia

(sample BB-DC-4) that have up to 63 % X-site vacancies and plot within the vacancy group (Fig. 3a). Typical values for X-site vacancy in the other samples are 10 % to 50 % (Fig. 4e). All samples have less than 20 cation % of Ca at the X site; calcium abundances are particularly low in tourmaline from the mineralized breccias. In the Al-Fe-Mg discrimination diagram of Henry & Guidotti (1985), data for the Blackbird tourmaline plot on the Al-rich side of the schorl-dravite join and cover a wide range of Fe/(Fe+Mg) values, from about 0.30 to 0.85 (Fig. 3b). Tourmaline data plot either within field 2 (Li-poor granitoids, pegmatites and aplites), field 4 (Al-saturated metapelites and metapsammites), or field 5 (metapelites and metapsammites lacking an Al-saturating phase). The wallrock-hosted tourmaline stands out compositionally from most other groups in this and other diagrams because of lower Fe/(Fe+Mg) and Na/(Na+Ca) values (Fig. 4a, see also 4d). At the other end of the compositional spectrum, with high Fe/(Fe+Mg) and high Na/(Na+Ca) values (low Ca and Mg contents), is the breccia-hosted tourmaline and that from the South Idaho stratabound ore zone (Figs. 4b, d). Tourmaline from the quartz veins and from the granite overlaps compositionally with the breccia-hosted tourmaline, but is distinguished from the latter by relatively high Al contents and low values for the X-site vacancy (Fig. 4e).

Most Blackbird tourmaline is more Al-rich than ideal schorl-dravite compositions (Figs. 3b, 4e), and the positive correlation of total Al with X-site vacancies (Fig. 4e) suggests that the "excess Al" (total Al > 6 apfu) is charge-balanced by the foitite-magnesiofoitite substitution, $(\square,Al)(Na,Fe)_{-1}$ or $(\square,Al)(Na,Mg)_{-1}$. Very few compositions have Al(Z) contents less than 6 apfu, which suggests minimal substitution of Fe^{3+} for Al. The exceptions to this include several grains from the granite-hosted quartz vein (sample 67SB160A) and one composition each from mineralized and barren tourmaline breccias from the CoNiCu locality (samples JS-06-32B and CoNiCu-tg). Negligible contents of ferric iron are also suggested by the lack of excess cation charge if all Fe is assumed as Fe^{2+}. Complete analyses would be needed to quantify the proportion of ferric to ferrous iron in the tourmaline but the microprobe data clearly suggest that it is low, which implies deposition from relatively reduced hydrothermal fluids.

Most Blackbird tourmaline has low Ti contents, less than 0.5 wt% TiO_2 (0.05 Ti apfu, see Fig. 4c), with scattered higher values in some samples but little dependency on host lithology. The fluorine

concentrations in most samples are below the detection limit (0.04 wt %). Exceptions to this pattern are tourmalines from the megacrystic granite (samples SA 1-3, SA 1-4) and the granite-hosted quartz vein (sample 67SB160A), which typically have F concentrations of 0.1 to 0.2 wt % F (Table 1). Only one sample from outside the granite, in the stratabound ore zone of the South Idaho deposit (sample GH-BB-20), has appreciable fluorine contents in tourmaline, and in this case, it is only the rims of zoned grains that contain 0.07 to 0.18 wt % F. These F contents are low relative to those in tourmaline from many other hydrothermal ore deposits (up to 1.9 wt %, Taylor & Slack 1984, Sinclair & Richardson 1992, Williamson *et al.* 2000, Mlynarczyk & Williams-Jones 2006). Together with the absence of fluorite or other F-rich minerals in the deposits, the tourmaline data suggest that hydrothermal fluids in the Blackbird district had low F contents. Chlorine concentrations in tourmaline are, without exception, below the detection limit of 0.02 wt %. Even tourmalines from wallrock samples SS-1A-456 and RO5-03-419, which have abundant Cl-rich biotite, contain only negligible Cl.

Compositional zoning was evaluated in all samples and determined to be weak, patchy, or absent in most wallrock- and granite-hosted tourmaline, but relatively common and locally strong in some tourmaline from the breccias and stratabound ores. Typically, the rims of zoned grains are enriched in Mg, Ca, and Ti, and are depleted in Fe and Al, relative to the cores (Fig. 5a-c). A special case of strong compositional zoning was found in mineralized sample SP-79-803, which is a Co-rich metasedimentary rock (argillite) from the stratabound Brown Bear ore zone. Most tourmaline in this sample forms small and unzoned (<50 μm) prismatic grains but the interesting feature are larger crystals that have optically distinct cores. Three such zoned grains occur in the thin section studied; the following arguments suggest that the cores are detrital in origin. First, the core compositions differ in terms of Mg, Fe, Al, Ti, and Ca contents whereas rims in all three grains are nearly the same (Fig. 5d-f). Note also that the compositional shift from core to rim in SP-79-803 is opposite that observed in other samples from the Blackbird district (compare Fig. 5a-c), which underscores the point that these core compositions are exotic. Second, some cores are irregular in form and not concentric with the outer grain shape. Third, and this is brought up in the following section, there is a strong and abrupt contrast in boron isotope composition between cores and rims, and the rim compositions are in the same range as the unzoned tourmaline in this sample.

343

344 ***Boron isotope compositions***

345 Table 3 summarizes the range, mean value, and standard deviation of B-isotope compositions
346 determined on tourmaline from the Blackbird district (for all results see electronic supplement ESM
347 Table 1). The total range of $\delta^{11}B$ values is very large, from -21.7 to +3.3‰ (Fig. 6). From 4 to 16
348 analyses were made in each sample, depending on the petrographic complexity and abundance of
349 tourmaline. Isotopic variations within individual samples are mostly less than 5‰, and the standard
350 deviation of multiple analyses is rarely greater than the analytical uncertainty of 2‰ (Table 3). All
351 optically zoned grains were checked for isotopic zoning by multiple SIMS analyses. Some grains
352 show internal variations in $\delta^{11}B$ greater than the 2‰ uncertainty, but variations tend to be patchy (Fig.
353 7d, e). The single case of systematic core-to-rim isotopic zoning is that of sample SP-79-803 having
354 the detrital cores described above. The cores in the three grains measured (A, B, C on Fig. 5d-f) are
355 not all uniform in isotopic composition: core compositions from two grains are among the lowest in
356 the entire data set, at -21.1, -20.5, and -20.0‰. The core in a third grain is much different isotopically,
357 at -5.7‰. The tourmaline rims in these grains range in composition from -7.5 to -3.9‰, which is close
358 to the value of unzoned tourmaline in this sample (-5.9‰). The variability in core compositions and
359 the extreme isotopic contrast of more than 13‰ between core and rim compositions in these grains
360 support other evidence for a detrital origin of the cores in this sample. Marschall *et al.* (2008)
361 described isotopically variable detrital cores in tourmaline from Syros, Greece, whose chemical and
362 isotopic distinction from their rims survived subsequent metamorphism.

363 From the frequency distribution of B-isotope ratios we distinguish isotopically light and heavy
364 groups of tourmaline from the Blackbird district, with a boundary between the two at about -8‰ (Fig.
365 6). Among the isotopically light tourmaline grains are those from the megacrystic granite (average -
366 16.9 ± 2.0 ‰) and the granite-hosted quartz-tourmaline vein (average -13.1 ± 3.4‰). Other members
367 of this group are the siltite-hosted quartz-tourmaline vein from the Ram deposit (average -12.8 ±
368 2.2‰) and tourmaline in wallrocks to the Ram and Sunshine deposits (average -9.9 ± 1.7‰ and -9.4 ±
369 2.2‰, respectively). Palmer & Slack (1989) determined a $\delta^{11}B$ value of -8.14‰ for fine-grained
370 tourmaline in a stratabound tourmalinite from the hangingwall of the Brown Bear deposit. This value

371 is in good agreement with our results for the wallrock tourmaline. The tourmaline group having
372 relatively heavy B-isotope compositions includes that in the stratabound ore zone at the South Idaho
373 deposit (average -1.2 ± 3.0‰), and all breccia-hosted tourmaline regardless of location, form, or
374 association with or without sulfide mineralization. In detail, tourmalines in the mineralized breccia
375 pipes at the Haynes-Stellite and the CoNiCu deposits average +0.1 ± 0.7‰ and +0.3 ± 1.0‰,
376 respectively; tourmaline from mineralized breccia in the Idaho stratabound ore zone averages -0.1 ±
377 2.7‰. Tourmaline from barren breccia pipes at CoNiCu and Beliel have average $\delta^{11}B$ values of -4.7 ±
378 2.2 ‰ and +1.6 ± 1.7‰, respectively. The average for tourmaline from the unmineralized quartzite
379 breccia east of the district is -2.5 ± 2.0‰.
380 We took care to locate SIMS analyses close to the electron microprobe spots to permit comparison
381 of chemical and B-isotope compositions. No systematic relationships in the Blackbird tourmalines
382 were found. A lack of correlation between major-element concentrations and B-isotope compositions
383 in tourmaline has been noted in other studies (*e.g.*, Jiang & Palmer 1998, Krienitz *et al.* 2008).
384
385 **DISCUSSION**
386 ***Controls on compositional variations in tourmaline***
387 The considerable range of tourmaline compositions in the Blackbird district with respect to major
388 elements depends in part on the host-rock lithology. For example, dravitic tourmaline, with Fe/(Fe +
389 Mg) < 0.5, is almost exclusively found in samples of biotite-rich wallrock (Fig. 4a). Also, fluorine
390 concentrations above the detection limit are restricted to tourmaline from the granite or quartz veins
391 within the granite. Granite-hosted tourmaline is also distinctive in having high total Al and moderate
392 X-site vacancies (Fig. 4e). Some of the observed range of chemical compositions is due to zonation
393 (Fig. 5). Typically, the rims of zoned tourmaline grains show a relative increase in Mg, Ti, and Ca at
394 the expense of Fe and Al. These trends presumably reflect changing concentrations in the
395 hydrothermal fluids or changes in the mineral assemblage (*e.g.*, Fe uptake during pyrite
396 crystallization), but their interpretation is complicated by the possible polymetamorphic history of the
397 district.

There was significant recrystallization of the Blackbird deposits during Cretaceous metamorphism, which is best demonstrated by Cretaceous Lu-Hf ages of metamorphic garnet in silicate wallrocks, by Cretaceous U-Pb ages of monazite from the sulfide zones, and by the widespread occurrence of coarse euhedral cobaltite grains in the deposits (Zirakparvar *et al.* 2007, Aleinikoff *et al.* 2011, Slack 2011). With respect to tourmaline, a contrast in textures and grain sizes is also attributed to the recrystallization process. Thus, in most samples from the stratabound sulfide deposits, wallrocks, and breccias, tourmaline forms a fine-grained (10-50 μm) mosaic of subhedral to anhedral crystals that we interpret as primary, Mesoproterozoic growth of tourmaline. Other samples contain coarser (>0.5 mm) euhedral tourmaline, which we attribute to recrystallization during later hydrothermal or metamorphic events. An example is the coarse-grained tourmaline occurring in undeformed quartz veins within wallrocks at the Ram deposit (sample R97-15-221). We propose that the formation of these and similar tabular veins relates to the Cretaceous event, and note that the contained tourmaline has similarly high Mg, Ti, and Ca concentrations, as do the rims of zoned tourmaline grains in many of the other samples. The Cretaceous recrystallization of tourmaline in the Blackbird district is relevant for interpretion of the B-isotope data discussed below.

Boron isotope variations and implications for multiple sources

First-order features of the boron isotope data from the Blackbird tourmaline are the large overall range of compositions (-21.7 to +3.3‰) and the contrast between tourmaline from metamorphic wall rocks, quartz veins, and granite (low $\delta^{11}B$ group) versus tourmaline from the stratabound ore and breccia zones (high $\delta^{11}B$ group). The total range in $\delta^{11}B$ values of 25‰ and the systematic relationship between isotopic composition of tourmaline and its lithologic host are inconsistent with a single boron source for the district. Instead, the results suggest that at least two discrete sources of boron, and, by inference, at least two sources of fluid, were present during tourmaline growth in the Blackbird district. This conclusion ignores the detrital tourmaline cores in sample SP-79-803, which represent a separate and earlier phase of tourmaline growth unrelated to the Blackbird mineralization and Cretaceous recrystallization events.

Before discussing the tourmaline data in terms of boron sources, it is necessary to consider the temperature-dependent fractionation of ^{11}B and ^{10}B between tourmaline and hydrothermal fluid, which can be significant. Different values for the fractionation factors have been experimentally determined by Palmer *et al.* (1992) and Meyer *et al*. (2008). The latter are preferred because of their success in modelling isotopic zoning profiles of synthetic tourmaline produced at known temperature and fluid composition (Marschall *et al.* 2009). The temperature of mineralization at Blackbird is poorly constrained. A reconnaissance fluid inclusion study obtained 275° to 375°C for high-salinity fluid (halite ± other daughter minerals) in quartz within the stratabound sulfide zones (Nash & Hahn, 1989). However, the fluid inclusion paragenesis in that study is uncertain, both with respect to sulfide mineralization and tourmaline formation. Lacking better temperature estimates for Blackbird tourmaline, we draw analogy to the 250° to 300°C estimates determined by Taylor *et al.* (2000) for footwall tourmalinites at the Mesoproterozoic Sullivan deposit. Using 300°C as a reasonable estimate for tourmaline formation in the Blackbird district, the hydrothermal fluid would be about 4‰ heavier in $\delta^{11}B$ than coexisting tourmaline based on Meyer *et al.* (2008). A 50°C misjudgement in the temperature of tourmaline growth corresponds to a relatively minor 0.7‰ difference in the fractionation effect.

Significance of the isotopically heavy tourmaline

Tourmaline having relatively high $\delta^{11}B$ values (the "heavy group") occurs exclusively in the stratabound sulfide deposits and tourmaline breccias, both mineralized and barren. Within this group, there is a small but intriguing contrast in $\delta^{11}B$ values between mineralized and barren tourmaline breccias in the CoNiCu deposit. Tourmaline from paragenetically early, mineralized (Co-rich) breccia is heavier (JS-06-32B, $\delta^{11}B$ -1.2 to +1.2‰) than later, barren tourmaline breccia (CoNiCu-tg, $\delta^{11}B$ -6.4 to -2.1‰). It is unclear if this difference is significant geologically, because the CoNiCu deposit is the only one where such a comparison of mineralized and barren breccias can be made, and because tourmaline from barren breccia at Beliel has even heavier boron than the mineralized CoNiCu breccia (AB-1-Beliel, $\delta^{11}B$ -0.9 to +3.2‰). An important observation is that tourmaline from both stratabound and breccia-hosted mineralization in the district belongs to the isotopically heavy group, and we

suggest this is evidence for a genetic link between the two. Equally important, the high end of $\delta^{11}B$ values from this tourmaline group implies a marine affinity for the boron. The calculated $\delta^{11}B$ values for the mineralizing fluid are as high as +7‰, based on the fractionation factor of about 4‰ at 300°C (Meyer et al., 2008). This exceeds the range of all major continental boron sources (sediments and clastic metasediments, granites, nonmarine evaporites), which have more negative $\delta^{11}B$ values (Palmer & Swihart 1996, Kasemann *et al.* 2000; Marschall & Ludwig, 2006). The known ranges in $\delta^{11}B$ values for siliciclastic marine sediments, arc volcanic rocks, and oceanic crust are commonly negative or slightly positive, but rarely as high as +7‰ (Palmer & Swihart 1996, Jiang *et al.* 1999, Peacock & Hervig 1999, Nakano & Nakamura 2001). According to data from Jiang *et al.* (2000), the fine-grained, clearly pre-metamorphic tourmalinite from the Sullivan area and elsewhere in the Belt and Purcell Supergroups of the northern Rocky Mountains is uniformly lower than -2.3‰ in $\delta^{11}B$. Given these constraints, the most viable source for the high $\delta^{11}B$ values of Blackbird tourmaline is marine evaporites, carbonates, or entrained seawater. This is consistent with the presence of high Cl contents in biotite within biotite-rich wallrocks to the sulfide deposits (Nash & Connor 1993). The Yellowjacket Formation, which is broadly coeval with the Apple Creek Formation, locally contains marine carbonate beds and scapolite-bearing and tourmaline-rich schists, which have been interpreted as meta-evaporites (Tysdal & Desborough 1997, Tysdal *et al.* 2003). We propose that leaching of marine-sourced boron from these or similar lithologies in the Mesoproterozoic metasedimentary sequences is the best explanation for the heavy group of Blackbird tourmaline. The isotopically "heavy group" of tourmaline samples is distinct but not homogeneous, and has $\delta^{11}B$ values as low as -6.9‰ (Fig. 6). To what extent this range in isotopic composition records variations in temperature of mineralization or fluid:rock ratios, or mixing of fluids from different B sources, cannot be evaluated with certainty at present.

Significance of the isotopically light tourmaline

The isotopically light group includes tourmaline from the megacrystic granite, quartz veins hosted by the granite and by siltite (the last probably Cretaceous), and from the biotite-rich wallrocks of the Apple Creek Formation at the Sunshine and Ram deposits (Fig. 6). The isotopic composition of

tourmaline from the megacrystic granite and quartz vein within it (-21 to -10‰) is important as an indicator for the expected isotopic composition of boron in a local magmatic-hydrothermal fluid. Since only minor fractionation is expected between tourmaline and high-temperature fluid (e.g., 1‰ at 600°C, Meyer *et al.* 2008), we can infer that granite-sourced boron in the Blackbird district would have had $\delta^{11}B$ values of about -15 ±5‰. Magmatic-hydrothermal fluid with this composition is clearly unimportant as a boron source for the stratabound and breccia-hosted mineralized tourmaline (heavy group), but it may have played a role in the wallrock-hosted tourmaline. Wallrock tourmaline in the Ram and Sunshine deposits (RO5-03-419 and SS-1A-456, respectively) have almost identical $\delta^{11}B$ ranges of -12.7 to -7.6‰ and -13.0 to -7.6‰ (Table 3), which overlap at their low end with that of the magmatic-hydrothermal fluid. Similarity in composition between the Ram and Sunshine tourmaline has signficance because they are texturally very different. The sample from the Sunshine deposit contains disseminated, fine-grained tourmaline (0.1 mm maximum length), suggesting a primary (pre-metamorphic) growth, whereas tourmaline in wallrock at the Ram deposit is much coarser (1 to 3 mm) likely due to metamorphic recrystallization of primary tourmaline. If this interpretation is correct, the similar $\delta^{11}B$ values of the two tourmaline samples suggest that recrystallization had little effect on the B-isotopic composition, implying that the metamorphic fluid and earlier hydrothermal fluid(s) had a similar boron isotopic composition. We can estimate the composition of Cretaceous metamorphic fluids from the $\delta^{11}B$ values of tourmaline in the post-mineralization quartz veins in siltite at the Ram deposit (sample R97-15-221), which are interpreted to have formed during that event. This coarse (1-3 mm) tourmaline has variable but light $\delta^{11}B$ values (-17.0 to -9.2‰) in the same range as other tourmalines in the "light group." Therefore, Cretaceous metamorphic fluids appear not to have had a distinctive B-isotope composition compared to the granite and the Mesoproterozoic metasedimentary rocks of the Apple Creek Formation.

If we take the $\delta^{11}B$ range of disseminated and fine-grained tourmaline in the Sunshine deposit wall rocks (-13 to -7.6‰) as the primary pre-metamorphic composition, a fitting boron source could be marine clays in the footwall siliciclastic sediments. Jiang *et al.* (1999, 2000) also proposed a marine clastic sedimentary source of boron to explain similar B-isotope values of tourmalinites from the Sullivan deposit, British Columbia, and from other tourmalinites within the Belt-Purcell basin. Those

authors, however, required an additional component of isotopically lighter boron to explain all of the tourmaline data and they proposed an additional contribution from non-marine evaporates in the basin. Our results suggest that in the Blackbird district a granite-derived magmatic-hydrothermal fluid could be an alternative source of isotopically light boron.

Like the isotopically heavy group of tourmaline, the light group spans a considerable range of $\delta^{11}B$ values. One can speculate that part of this variation is due to mixing between the light and heavy boron (fluid) sources, which might be viable for the wallrock samples adjacent to mineralization. However, mixing is unlikely to be the sole explanation because other factors influence the isotopic composition of tourmaline, including temperature-dependent fractionation, variations in fluid : rock ratios, and Rayleigh fractionation (Jiang *et al.* 1999). The metamorphic overprint on the Blackbird ores and wallrocks can also contribute to isotopic variations although the effect is probably not large as discussed above. The separate contributions of these different factors are impossible to evaluate rigorously without more information on mineralization temperatures and fluid compositions.

Implications for metallogenesis

Of obvious interest for economic geology and mineral exploration is the question of whether tourmaline in the Blackbird district shows systematic features in major element or isotopic composition that could indicate the presence or absence of associated metal (*e.g.,* Co, Cu, Au) enrichments. Jiang *et al.* (2000) discussed this point in their study of tourmaline from the Sullivan massive sulfide deposit and from regional tourmalinites in lower siliciclastic strata of the Mesoproterozoic Belt and Purcell Supergroups. Their data indicate that tourmaline from Sullivan and other massive sulfide deposits within these strata tends to have high ratios of Mg/(Mg + Fe), but that this general pattern is not a robust indicator of associated mineralization (see also Slack 1996). The association of Mg-rich tourmaline with mineralization does not in any case hold for the Blackbird district, where the most magnesian tourmaline occurs in biotite-rich wallrocks with no directly related metal enrichments, and in barren and postore quartz-tourmaline veins of probable Cretaceous age. Indeed, tourmaline from the stratabound sulfide deposits and mineralized breccias in the Blackbird district are among the most Fe-rich of all samples in the suite (see Fig. 4d).

In terms of major elements determined in this study, there are no obvious compositional differences between mineralized and unmineralized samples that might have exploration significance. However, the B-isotope compositions of tourmaline from the mineralized zones are distinctive. Tourmaline in mineralized samples from the Haynes-Stellite, CoNiCu, and South Idaho deposits all have moderately negative to positive $\delta^{11}B$ values, which contrast greatly with the strongly negative values in tourmaline from the metasedimentary rocks of the Apple Creek Formation and from the megacrystic granite (Fig. 6). The inferred B-isotopic composition of hydrothermal fluid in the Blackbird stratabound and breccia-hosted deposits (4‰ heavier than tourmaline) reaches $\delta^{11}B$ values up to about +7‰. The upper range of these values implies a major contribution of marine-sourced boron in the fluid, most likely from meta-carbonate or meta-evaporite layers in the broadly coeval Yellowjacket Formation.

There is conflicting evidence for the role of granite-derived fluid in the Blackbird district. A granitic contribution is permitted in the case of the light B-isotope values of pre-metamorphic, fine–grained tourmaline from the Sunshine deposit wallrocks; a magmatic or mantle source of helium is implied from the highly-radiogenic He-isotope values (R/Ra = 8) of fluid inclusions from paragenetically early quartz in the Sunshine deposit (Johnson *et al*. 2007). On the other hand, Bookstrom *et al.* (2007) and Johnson *et al.* (2007) reported sulfide $\delta^{34}S$ values from +7 to +9‰ for the Blackbird ores and noted that these results are consistent with a sedimentary sulfur source, but not with a purely magmatic-hydrothermal, sulfur source. We emphasize, however, that the source of metals in the deposits is not necessarily the same as the sources of light elements such as B, He, and S. Considering the distinctive association of metals concentrated in the Blackbird deposits (Co, Cu, Au, Bi, REE, Y, Be), it is likely that some—especially Bi, REE, Y, and Be—were derived from the megacrystic granite (Slack 2011). The issue is nevertheless unresolved and future studies involving radiogenic isotopes (*e.g.*, Nd, Sr, Pb) and other stable isotopes (*e.g.*, C, O) could provide valuable insights into the nature and contribution of these source reservoirs during mineralization in the Blackbird district.

ACKNOWLEDGEMENTS

In this study we relied on the generous donation of tourmaline samples by colleagues to whom we are very grateful, including A.A. Bookstrom, S.E. Box, J.T. Nash, and S.G. Peters of the U.S. Geological Survey; K.R. Chamberlain of the University of Wyoming; and G.R. Hughes and G.A. Hahn formerly of Noranda Exploration, Inc. Discussions with A.A. Bookstrom have been especially helpful. We also thank W.G. Scales, G. King, and Formation Metals, Inc. (previously Formation Capital Corp.) for providing access to their properties in the district and to drill cores for sampling. Thanks to I. Schaepan for her able assistance with SIMS analyses in Potsdam. Suggestions and constructive reviews by USGS colleagues A.A. Brookstrom, C.A. Johnson, and R.R. Seal, II, journal referees S.-Y. Jiang and anonymous, guest editor Horst Marschall, and CM editor Robert Martin are kindly acknowledged.

REFERENCES

ALEINIKOFF, J.N., SLACK, J.F., LUND, K.I., EVANS, K.V., MAZDAB, F.K., PILLARS, R.M. & FANNING, C.M. (2011): Constraints on the timing of Co-Cu±Au mineralization in the Blackbird district, Idaho, using SHRIMP U-Pb ages of monazite and xenotime plus zircon ages of related Mesoproterozoic orthogneiss and metasedimentary rocks. *Econ. Geol.* (in review).

ANDERSON, A.L. (1947): Cobalt mineralization in the Blackbird district, Lemhi County, Idaho. *Econ. Geol.* **42**, 22-46.

ARMSTRONG, J.T. (1995): CITZAF: a package of correction programs for the quantitative electron microbeam X-ray analysis of thick polished materials, thin films, and particles. *Microbeam Anal.* **4**, 177-200.

BARTH, S. (1993): Boron isotope variations in nature: a synthesis. *Geol. Rundschau* **82**, 640-651.

BEBOUT, G.E. & NAKAMURA, E. (2003): Record in metamorphic tourmalines of subduction-zone devolatilization and boron cycling. *Geology* **31**, 407-410.

BENDING, J.S. & SCALES, W.G. (2001): New production in the Idaho cobalt belt: a unique metallogenic province. *Inst. Mining Metall. Trans.* **110(B)**, B81-B87.

592 BOOKSTROM, A.A., JOHNSON, C.A., LANDIS, G.P. & FROST, T.P. (2007): Blackbird Fe-Cu-Co-
593 Au-REE deposits. *U.S. Geol. Survey Open-File Rept.* **2007-1280B**, 11-20
594 [http://pubs.usgs.gov/of/2007/1280/].
595 CANTANZARO, E.J., CHAMPION, C., GARNER, E., MARINENKO, G., SAPPENFIELD, K. &
596 SHIELDS, W. (1970): Boric acid: isotopic and assay standard reference materials. *National Bur.*
597 *Standards (U.S.) Spec. Publ.* **260**.
598 CHAUSSIDON, M. & ALBARÈDE, F. (1992): Secular boron isotope variations in the continental
599 crust: an ion microprobe study. *Earth Planet. Sci. Lett.* **108**, 229-241.
600 DOUGHTY, P.T. & CHAMBERLAIN, K.R. (1996): Salmon River arch revisited: new evidence for
601 1370 Ma rifting near the end of deposition of the Middle Proterozoic Belt basin. *Can. J. Earth Sci.*
602 **33**, 1037-1052.
603 DOUGHTY, P.T. & CHAMBERLAIN, K.R. (2008): Protolith age and timing of Precambrian
604 magmatic and metamorphic events in the Priest River Complex, northern Rockies. *Can. J. Earth*
605 *Sci.* **45**, 99-116.
606 DYAR, M.D., WIEDENBECK, M., ROBERTSON, D., CROSS, L.R., DELANY, J.S., FERGUSON,
607 K., FRANCIS, C.A., GREW, E.S., GUIDOTTI, C.V., HERVIG, R.L., HUGHES, J.M., HUSLER,
608 J., LEEMAN, W.P., MCGUIRE, A.V., RHEDE, D., ROTHE, H., PAUL, R.L., RICHARDS, I. &
609 YATES, M. (2001): Reference minerals for microanalyses of light elements. *Geostandard.*
610 *Newslett.* **25**, 441-463.
611 EISEMAN, H.H. (1988): *Ore geology of the Sunshine cobalt deposit, Blackbird mining district, Idaho*.
612 M.S. thesis, Colorado School of Mines, Golden, Colorado, U.S.A., 191 pp.
613 EVANS, K.V. (1986): Middle Proterozoic deformation and plutonism in Idaho, Montana and British
614 Columbia. *In* Belt Supergroup: A Guide to Proterozoic Rocks of Western Montana and Adjacent
615 Areas (Roberts, S.M., ed.). *Montana Bur. Mines Geol. Spec. Publ.* **94**, 237-244.
616 EVANS, K.V., NASH, J.T., MILLER, W.R., KLEINKOPF, M.D. & CAMPBELL, D.L. (1995):
617 Blackbird Co-Cu deposits. *U.S. Geol. Survey Open-File Rept.* **95-831**, 145-151.GARDA, G.M,
618 TRUMBULL, R.B., BELJAVSKIS, P. & WIEDENBECK, M. (2009): Boron isotope composition

of tourmalinite and vein tourmalines associated with gold mineralization, Serra do Itaberaba Group, central Ribeira belt, SE Brazil. *Chem. Geol.* **264**, 207-220.

GONFIANTINI, R., TONARINI, S., GRÖNING, M., ADORNI-BRACCESI, A., AL-AMMAR, A.S., ASTNER, M., BAECHLER, S., BARNES, R.M., BASSETT, R.L., COCHERIE, A., DEYHLE, A., DINI, A., FERRARA, G., GAILLARDET, J., GRIMM, J., GUERROT, C., KRAEHENBUEHL, U., LAYNE, G., LEMARCHAND, D., MEIXNER, A., NORTHINGTON, D.J., PENNISI, M., REITZNEROVA, E., RODUSHKIN, I., SUGIURA, N., SURBERG, R., TONN, S., WIEDENBECK, M., WUNDERLI, S., XIAO Y.-K. & ZACK, T. (2003): Intercomparison of boron isotope and concentration measurements. Part II: Evaluation of Results. *Geostandard. Newslett.* **27**, 41-57.

HAWTHORNE, F.C. & HENRY, D.J. (1999): Classification of the minerals of the tourmaline group. *Eur. J. Mineral.* **11**, 201-215.

HENRY, D.J. & DUTROW, B.L. (1996): Metamorphic tourmaline and its petrologic applications. *In* Boron: Mineralogy, Petrology and Geochemistry. (E.S. Grew & L.M. Anovitz, eds.). *Rev. Mineral.* **33**, 502-558.

HENRY, D.J. & GUIDOTTI, C.V. (1985): Tourmaline as a petrogenetic indicator mineral: an example from the staurolite-grade metapelites of NW Maine. *Am. Mineral.* **70**, 1-15.

JIANG, S.-Y. & PALMER, M.R. (1998): Boron isotope systematics of tourmaline from granites and pegmatites: a synthesis. *Eur. J. Mineral.* **10**, 1253-1265.

JIANG, S.-Y., PALMER, M.R., SLACK, J.F. & SHAW, D.R. (1999): Boron isotope systematics of tourmaline formation in the Sullivan Pb–Zn–Ag deposit, British Columbia, Canada. *Chem. Geol.* **158**, 131-144.

JIANG, S.-Y., PALMER, M.R., SLACK, J.F. & ANDERSON, D. (2000): Chemical and boron isotope compositions of tourmaline from massive sulphide deposits and tourmalinites in the Mesoproterozoic Belt and Purcell Supergroups, southeastern British Columbia and northwestern Montana. *In* The Geological Environment of the Sullivan Deposit, British Columbia (J.W. Lydon, T. Höy, J.F. Slack & M.E. Knapp, eds.). *Geol. Assoc. Can., Mineral Deposits Div, Spec. Publ.* **1**, 336-354.

JIANG, S.-Y., PALMER, M.R. & YEATS, C.J. (2002): Chemical and boron isotopic compositions of tourmaline from the Archean Big Bell and Mount Gibson gold deposits, Murchison Province, Yilgarn craton, Western Australia. *Chem. Geol.* **188**, 229-247.

JOHNSON, C.A., LANDIS, G. & BOOKSTROM, A.A. (2007): Sulfur and helium isotopes in the cobalt+copper±gold deposits of the Idaho cobalt belt. *Geol. Soc. Am., Abstr. Programs* **39**, 412.

KASEMANN, S., ERZINGER, J. & FRANZ, G. (2000): Boron recycling in the continental crust of the central Andes from the Palaeozoic to Mesozoic, NW Argentina. *Contrib. Mineral. Petrol.* **140**, 328-343.

KRIENITZ, M.-S., TRUMBULL, R.B., HELLMANN, A., KOLB, J., MEYER, F.M. & WIEDENBECK, M. (2008): Hydrothermal gold mineralization at the Hira Buddini gold mine, India: constraints on fluid sources and evolution from boron isotopic compositions of tourmaline. *Min. Deposita* **43**, 421-434.

LUND, K.I. & TYSDAL, R.G. (2007): Stratigraphic and structural setting of sediment-hosted Blackbird gold-cobalt-copper deposits, east-central Idaho, U.S.A. *In* Proterozoic Geology of Western North America and Siberia (P.K. Link & R.S. Lewis, eds.). *Soc. Econ. Paleon. Mineral., Spec. Publ.* **86**, 129-147.

LUND, K., ALEINIKOFF, J.N., EVANS, K.V., DU BRAY, E.A., DEWITT, E.H. & UNRUH, D.M. (2010): SHRIMP U-Pb dating of recurrent Cryogenian and Late Cambrian-Early Ordovician alkalic magmatism in central Idaho: implications for Rodinian rift tectonics. *Geol. Soc. Am. Bull.* **122**, 430-453.

LUND, K., EVANS, K.V. & KUNK, M.J. (2007): Structural evolution of gold-bearing cobalt-copper deposits of the Blackbird mining district, east-central Idaho. *Geol. Soc. Am., Abstr. Programs* **39**, 535.

MARSCHALL, H.R. & LUDWIG, T. (2006): Re-examination of the boron isotopic composition of tourmaline from the Lavicky Granite, Czech Republic, by secondary ion mass spectrometry: back to normal. *Geochem. J.* **40**, 631-638.

MARSCHALL, H.R., ALTHERR, R., KALT, A. & LUDWIG, T. (2008): Detrital, metamorphic and metasomatic tourmaline in high-pressure metasediments from Syros (Greece): intra-grain boron

675 isotope patterns determined by secondary-ion mass spectrometry. *Contrib. Mineral. Petrol.* **155**,
676 703-717.
677 MARSCHALL, H.R., MEYER, C., WUNDER, B., LUDWIG, T. & HEINRICH, W. (2009):
678 Experimental boron isotope fractionation between tourmaline and fluid: confirmation from in situ
679 analyses by secondary ion mass spectrometry and from Rayleigh fractionation modelling.
680 *Contrib. Mineral. Petrol.* **158**, 675-681.
681 MEYER, C., WUNDER, B., MEIXNER, A., ROMER, R.L. & HEINRICH, W. (2008): Boron-isotope
682 fractionation between tourmaline and fluid: an experimental re-investigation. *Contrib. Mineral.*
683 *Petrol.* **156**, 259-267.
684 MLYNARCZYK, M.S.J. & WILLIAMS-JONES, A.E. (2006): Zoned tourmaline associated with
685 cassiterite: implications for fluid evolution and tin mineralization in the San Rafael Sn-Cu
686 deposit, southeastern Peru. *Can. Mineral.* **44**, 347-365.
687 MODRESKI, P.J. (1985): Stratabound cobalt-copper deposits in the Middle Proterozoic Yellowjacket
688 Formation in and near the Challis quadrangle. *U.S. Geol. Survey Bull.* **1658**, 203-221.
689 NAKANO, T. & NAKAMURA, E. (2001): Boron isotope geochemistry of metasedimentary rocks and
690 tourmalines in a subduction zone metamorphic suite. *Phys. Earth Planet. Int.* **127**, 233-252.
691 NASH, J.T. (1989): Geology and geochemistry of synsedimentary cobaltiferous-pyrite deposits, Iron
692 Creek, Lemhi County, Idaho. *U.S. Geol. Survey Bull.* **1882**, 32 pp.
693 NASH, J.T. & CONNOR, J.J. (1993): Iron and chlorine as guides to stratiform Cu-Co-Au deposits,
694 Idaho cobalt belt, USA. *Min. Deposita* **28**, 99-106.
695 NASH, J.T. & HAHN, G.A. (1989): Stratabound Co-Cu deposits and mafic volcaniclastic rocks in the
696 Blackbird mining district, Lemhi County, Idaho. *In* Sediment-Hosted Stratabound Copper
697 Deposits (R.W. Boyle, A.C. Brown, C.W. Jefferson, E.C. Jowett & R.V. Kirkham, eds.). *Geol.*
698 *Assoc. Canada, Spec. Paper* **36**, 339-356.
699 NOLD, J.L. (1990): The Idaho cobalt belt, northwestern United States—A metamorphosed
700 Proterozoic exhalative ore district. *Min. Deposita* **25**, 163-168.

PAL, D.C., TRUMBULL, R.B. & WIEDENBECK, M. (2010): Chemical and boron isotope compositions of tourmaline from the Jaduguda U (-Cu-Fe) deposit, Singhbhum shear zone, India: implications for the sources and evolution of mineralizing fluids. *Chem. Geol.* **277**, 245-260.

PALMER, M.R. & SLACK, J.F. (1989): Boron isotopic composition of tourmaline from massive sulfide deposits and tourmalinites. *Contrib. Mineral. Petrol.* **103**, 434-451.

PALMER, M.R. & SWIHART, G.H. (1996): Boron isotope geochemistry: an overview. *In* Boron: Mineralogy, Petrology and Geochemistry (E.S. Grew & L.M. Anovitz, eds.). *Rev. Mineral.* **33**, 709-744.

PALMER, M.R., LONDON, D., MORGAN, VI, G.B. & BABB, H.A. (1992): Experimental determination of fractionation of $^{11}B/^{10}B$ between tourmaline and aqueous vapor: a temperature- and pressure-dependent isotopic system. *Chem. Geol*. **101,** 123-129.

PEACOCK, S.M. & HERVIG, R.L. (1999): Boron isotopic composition of subduction-zone metamorphic rocks. *Chem. Geol.* **160**, 281-290.

PESQUERA, A., TORRES-RUIZ, J., GIL-CRESPO, P.P. & JIANG, S.-Y. (2005): Petrographic, chemical and B-isotopic insights into the origin of tourmaline-rich rocks and boron recycling in the Martinamor antiform (central Iberian zone, Salamanca, Spain). *J. Petrol.* **46**, 1013-1044.

SINCLAIR, W.D. & RICHARDSON, J.M. (1992): Quartz-tourmaline orbicules in the Seagull batholith, Yukon Territory. *Can. Mineral.* **30**, 923-935.

SLACK, J.F. (1996): Tourmaline associations with hydrothermal ore deposits. *In* Boron: Mineralogy, Petrology and Geochemistry. (E.S. Grew & L.M. Anovitz, eds.). *Rev. Mineral.* **33**, 559-644.

SLACK, J.F. (2006): High REE and Y concentrations in Co-Cu-Au ores of the Blackbird district, Idaho. *Econ. Geol.* **101**, 275-280.

SLACK, J.F. (2011): Stratabound Fe-Co-Cu-Au-Bi-Y-REE deposits of the Idaho cobalt belt, USA: multistage hydrothermal mineralization in a magmatic-related iron oxide-copper-gold system. *Econ. Geol.* (in review).

SLACK, J.F., PALMER, M.R., STEVENS, B.P.J. & BARNES, R.G. (1993): Origin and significance of tourmaline-rich rocks in the Broken Hill district, Australia. *Econ. Geol.* **88**, 505-541.

SLACK, J.F., SHAW, D.R., LEITCH, C.H.B. & TURNER, R.J.W. (2000): Tourmalinites and coticules from the Sullivan Pb–Zn–Ag deposit and vicinity, British Columbia: geology, geochemistry, and genesis. *In* The Geological Environment of the Sullivan Deposit, British Columbia (J.W. Lydon, T. Höy, J.F. Slack & M.E. Knapp, eds.). *Geol. Assoc. Can., Mineral Deposits Div., Spec. Publ.* **1**, 736-767.

SMITH, M.P. & YARDLEY, B.W.D. (1996): The boron isotopic composition of tourmaline as a guide to fluid processes in the southwestern England orefield: an ion microprobe study. *Geochim. Cosmochim. Acta* **60**, 1415-1427.

SPERLICH, R., GIERÉ, R. & FREY, M. (1996): Evolution of compositional polarity and zoning in tourmaline during prograde metamorphism of sedimentary rocks in the Swiss Central Alps. *Am. Mineral.* **81**, 1222-1236.

TAYLOR, B.E. & SLACK, J.F. (1984): Tourmalines from Appalachian-Caledonian massive sulfide deposits: textural, chemical, and isotopic relationships. *Econ. Geol.* **79**, 1703-1726.

TAYLOR, B.E., PALMER, M.R. & SLACK, J.F. (1999): Mineralizing fluids in the Kidd Creek massive sulfide deposit, Ontario: evidence from oxygen, hydrogen, and boron isotopes in tourmaline. *In* The Giant Kidd Creek Volcanogenic Massive Sulfide Deposit, Western Abitibi Subprovince, Canada (M.D. Hannington & C.T. Barrie, eds.). *Econ. Geol. Monogr.* **10**, 389-414.

TAYLOR, B.E., TURNER, R.J.W., LEITCH, C.H.B., WATANABE, D.H. & SHAW, D.R. (2000): Oxygen and hydrogen isotope evidence for the origins of mineralizing and alteration fluids, Sullivan Pb-Zn mine and vicinity, British Columbia. *In* The Geological Environment of the Sullivan Deposit, British Columbia (J.W. Lydon, T. Höy, J.F. Slack & M.E. Knapp, eds.). *Geol. Assoc. Can., Mineral Deposits Div., Spec. Publ.* **1**, 652-672.

TONARINI, S., PENNISI, M., ADORNI-BRACCESI, A., DINI, A., FERRARA, G., GONFIANTINI, R., WIEDENBECK, M. & GRÖNING, M. (2003): Intercomparison of boron isotope and concentration measurements. Part I: Selection, preparation and homogeneity tests of the intercomparison materials. *Geostandard. Newslett.* **27**, 21-39.

754 TRUMBULL, R.B. & CHAUSSIDON, M. (1999): Chemical and boron isotopic composition of
755 magmatic and hydrothermal tourmalines from the Sinceni granite-pegmatite system in Swaziland.
756 *Chem. Geol.* **153**, 125-137.
757 TRUMBULL, R.B., KRIENITZ, M.-S., GOTTESMANN, B. & WIEDENBECK, M. (2008):
758 Chemical and boron-isotope variations in tourmalines from an S-type granite and its source rocks:
759 the Erongo granite and tourmalinites in the Damara belt, Namibia. *Contrib. Mineral. Petrol.* **155**,
760 1-18.
761 TRUMBULL, R.B., KRIENITZ, M.-S., GRUNDMANN, G. & WIEDENBECK, M. (2009):
762 Tourmaline geochemistry and $\delta^{11}B$ variations as a guide to fluid–rock interaction in the Habachtal
763 emerald deposit, Tauern window, Austria. *Contrib. Mineral. Petrol.* **157**, 411-427.
764 TYSDAL, R.G. & DESBOROUGH, G.A. (1997): Scapolitic metaevaporite and carbonate rocks of
765 Proterozoic Yellowjacket Formation, Moyer Creek, Salmon River Mountains, central Idaho. *U.S.*
766 *Geol. Survey Open-File Rept.* **97-268**, 28 pp.
767 TYSDAL, R.G., LUND, K.I. & EVANS, K.V. (2003): Geologic map of the western part of the
768 Salmon National Forest. *U.S. Geol. Survey Geol. Invest. Series Map* **I-2765**
769 [http://pubs.usgs.gov/imap/i-2765/].
770 VHAY, J.S. (1948): Cobalt-copper deposits in the Blackbird district, Lemhi County, Idaho. *U.S. Geol.*
771 *Survey Strategic Min. Invest. Prelim. Rept.* **3-219**, 26 pp.
772 WILLIAMSON, B.J., SPRATT, J., ADAMS, J.T., TINDLE, A.G. & STANLEY, C.J. (2000):
773 Geochemical constraints from zoned hydrothermal tourmalines on fluid evolution and Sn
774 mineralization: an example from fault breccias at Roche, SW England. *J. Petrol.* **41**, 1439-1453.
775 XAVIER, R.P., WIEDENBECK, M., TRUMBULL, R.B., DREHER, A.M., MONTEIRO, L.V.S.,
776 RHEDE, D., DE ARAÚJO, C.E.G. & TORRESI, I. (2008): Tourmaline B-isotopes fingerprint
777 marine evaporites as the source of high salinity ore fluids in iron oxide-copper-gold deposits,
778 Carajás mineral province (Brazil). *Geology* **36**, 743-746.
779 ZIRAKPARVAR, N.A., BOOKSTROM, A.A. & VERVOORT, J.D. (2007): Cretaceous garnet
780 growth in the Idaho cobalt belt: evidence from Lu-Hf geochronology. *Geol. Soc. Am., Abstr*
781 *Programs* **39**, 413.

ZIRAKPARVAR, N.A., VERVOORT, J.D., MCCLELLAND, W. & LEWIS, R.S. (2010): Insights into the metamorphic evolution of the Belt-Purcell basin: evidence from Lu-Hf garnet geochronology. *Can. J. Earth Sci.* **47**, 161-179.

Figure captions

Figure 1. Simplified geological map of the Idaho cobalt belt showing locations of major stratabound sulfide deposits and stratabound iron oxide deposits (modified from Slack 2006). Geology from Tysdal *et al.* (2003) and Lund & Tysdal (2007). Ages of the Apple Creek Formation and the megacrystic granite are from Aleinikoff *et al.* (2011). Locations of analyzed samples not shown on this map are the quartz-tourmaline vein from the margin of the megacrystic granite and the disseminated grains within this granite, which are ca. 6 and 8 km, respectively, northeast of the map. The Blackbird district comprises the cluster of deposits centered on the Blackbird mine (BB). Brown Bear and Merle deposits, which are not shown, are ~1400 m northwest and ~600 m northeast of the Idaho deposit, respectively (locations in Bookstrom *et al.* 2007).

Figure 2. Photomicrographs of tourmaline samples (all plane transmitted light). (a) fine-grained tourmaline intergrown with chlorite, muscovite, and cobaltite (black); ore zone sample GH-BB-20, South Idaho deposit, (b) coarse-grained tourmaline intergrown with biotite and minor garnet; wallrock sample RO5-03-419, Ram deposit, (c) coarse-grained tourmaline in late quartz vein from siltite wallrocks; sample R97-15-221, Ram deposit, (d) fine-grained tourmaline with quartz and cobaltite (black) in mineralized breccia of argillite; sample GH-BB-23, Haynes-Stellite deposit, (e) fine-grained tourmaline with chlorite and muscovite in pseudomorphs after K-feldspar; sample SA-1-4, megacrystic granite, (f) coarse tourmaline in granite-hosted quartz vein; sample 67SB160A, megacrystic granite.

Figure 3. Overview of Blackbird tourmaline in classification diagrams, in (a) based on groups defined by the principal constituents in the X-site after Hawthorne & Henry (1999); and in (b) based on cation proportions of total Al, Fe and Mg after Henry & Guidotti (1985), with labeled divisions according to tourmaline provenance as follows: (1) Li-rich granitoid pegmatites and aplites, (2) Li-poor granitoids, pegmatites and aplites, (3) Fe^{3+}-rich quartz-tourmaline rocks (altered

granitoids), (4) metapelites and metapsammites with Al-saturating phase, (5) metapelites and metapsammites lacking Al-saturating phase, (6) Fe^{3+}-rich quartz-tourmaline rocks, calc-silicate rocks and metapelites, (7) low-Ca meta-ultramafic rocks and Cr-V-rich metasediments, (8) meta-carbonates and meta-pyroxenites.

Figure 4. Selected features of Blackbird tourmaline composition illustrated in terms of (a) atomic ratios Fe/(Fe+Mg) versus Na/(Na+Ca), (b) Ca versus Mg, (c) Ca versus Ti, (d) Mg versus Fe, (e) total Al versus X-site vacancies, and (f) total Al versus Fe. All element concentrations are in atoms per formula unit (pfu). Possible tourmaline exchange vectors are shown in panels (e) and (f) (□ = site vacancy), see text for discussion.

Figure 5. Examples of compositional zoning in tourmaline from the Blackbird district, which is restricted to mineralized and breccia-hosted samples. Samples illustrated in left-side plots (a, b, c) are unmineralized breccia AB-1-Beliel, statabound ore GH-BB-20, and unmineralized breccia CoNiCu-tg. The right-side plots (d, e, f) illustrate the variable compositional shifts from core to rim in three grains (A, B, C) of stratabound ore sample SP-79-803. The cores in this sample are interpreted as detrital in origin (see text).

Figure 6. Frequency histogram of boron isotope compositions of tourmaline from the Blackbird district, shown separately for sample groups. Also shown in the upper panel (dotted circle) is a B-isotope value of fine-grained tourmaline from a stratiform tourmalinite a few hundred meters from the Beliel breccia-hosted deposit (Palmer & Slack 1989). The lower panel shows the range of B-isotope composition of relevant continental and marine boron reservoirs (Barth 1993, Chaussidon & Albarède 1992, Palmer & Swihart 1996, Kasemann *et al.* 2000, Marschall & Ludwig 2006).

Figure 7. Back-scattered electron images of selected tourmaline samples showing examples of internal compositional variation and position of SIMS analysis spots with $\delta^{11}B$ values (in ‰). (a) JS-06-32B, mineralized breccia, CoNiCu (b) AB-1-Beliel, barren tourmaline breccia, (c) SP-79-803, mineralized metasediment with detrital core, stratabound ore, Black Bear deposit, (d) RO5-03-419, biotite-rich wall rock (e) SA-1-4, megacrystic granite, (f) GH-BB-20, mineralized metasediment, stratabound ore, South Idaho deposit. Mineral labels: Ap, apatite; Bt, biotite (Fe-

and Cl-rich); Cbt, cobaltite; Chl, chlorite; Kfs, K-feldspar; Ms, muscovite; Py, pyrite; Qtz, quartz; Tur, tourmaline; Zrn, zircon.

Table captions

Table 1. Selected electron-microprobe compositions of tourmaline from different lithotypes in the Blackbird district.

Table 2. Example of B-isotope results on reference tourmalines

Table 3. Summary of boron isotope composition of tourmaline from the Blackbird district

Electronic Supplementary Material (ESM)

ESM Table 1. Full data set of electron-microprobe and SIMS B-isotope compositions of tourmaline from the Blackbird district.

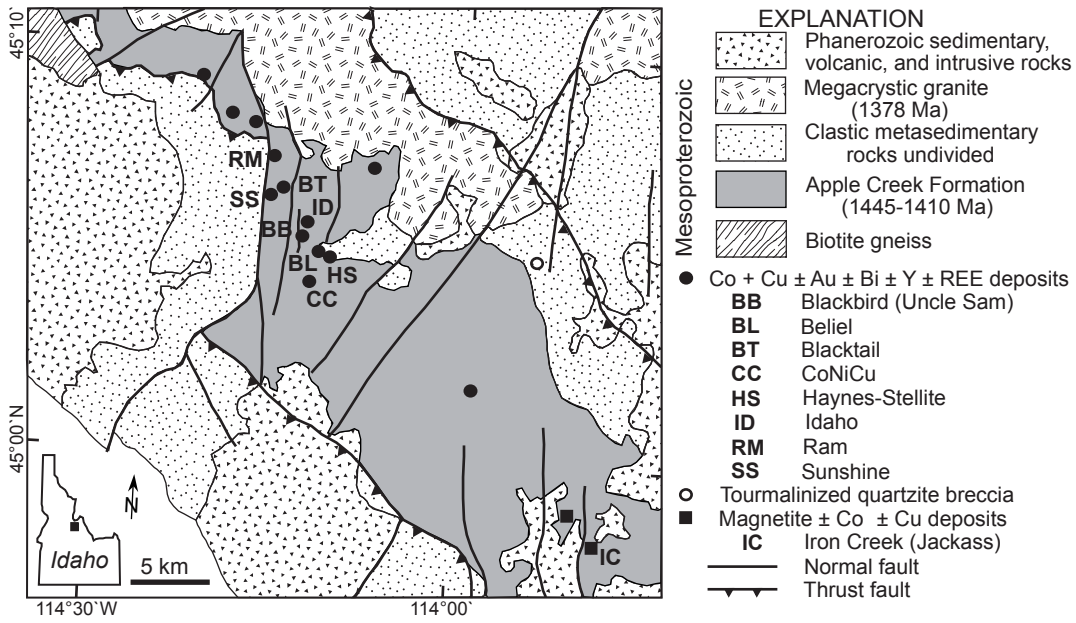

Trumbull et al. - Figure 1

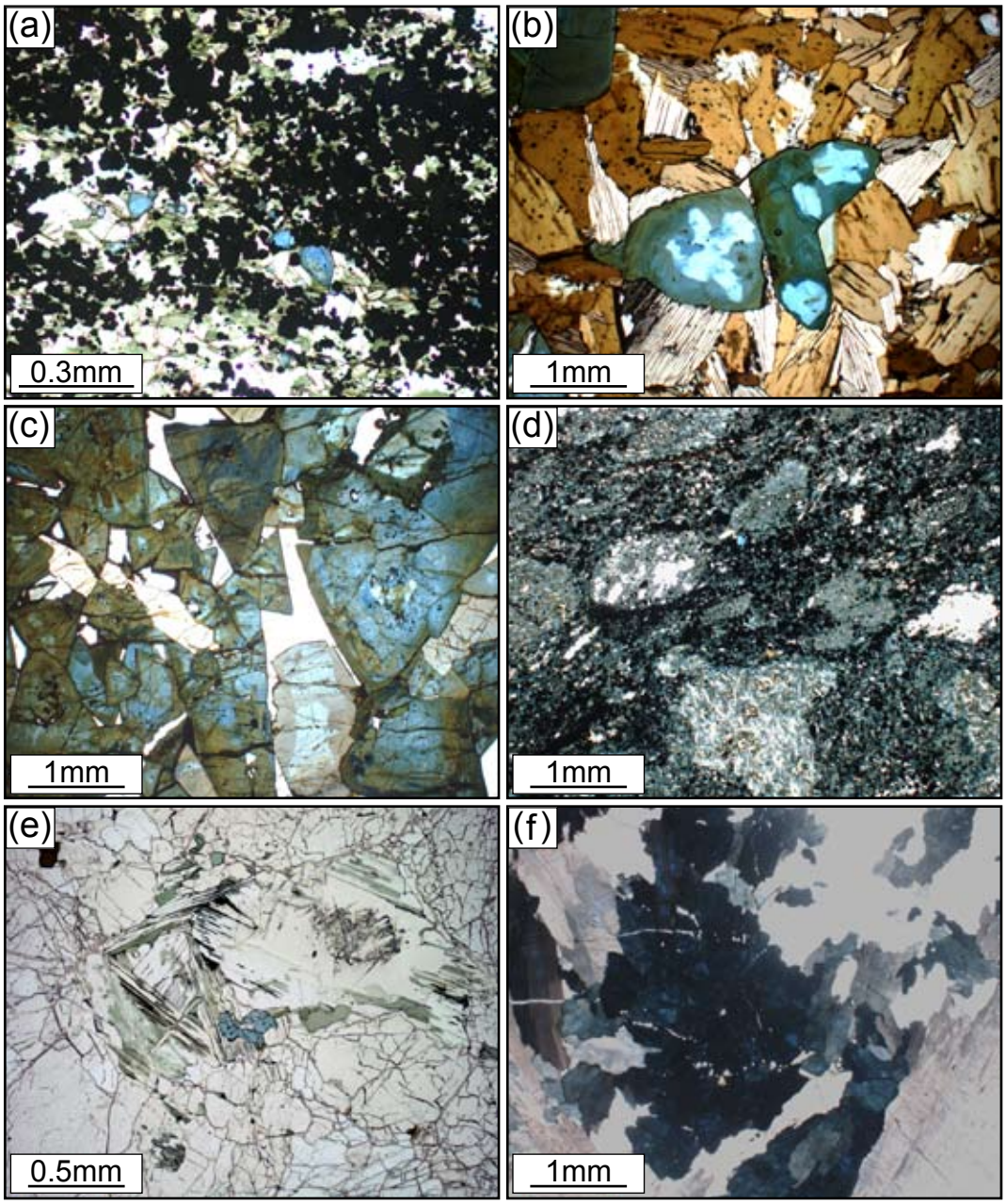

Trumbull et al. - Figure 2

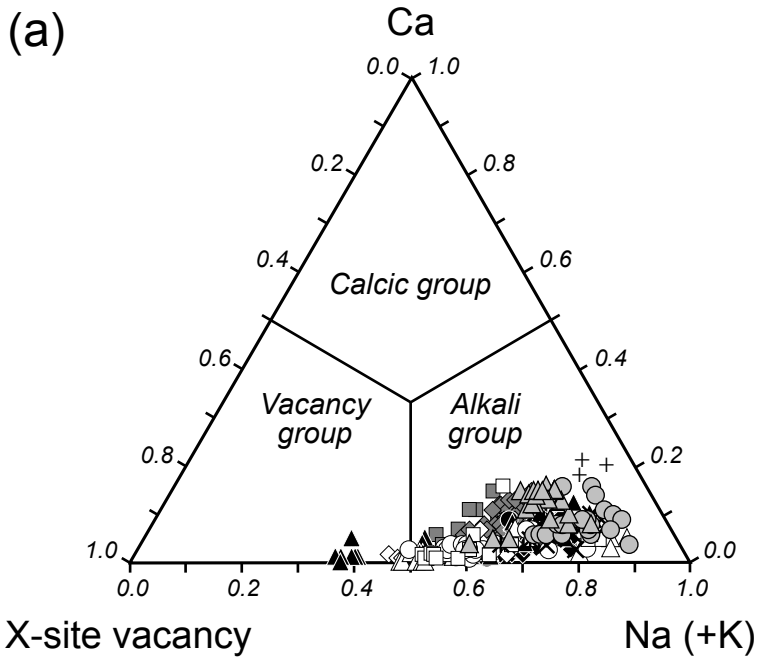

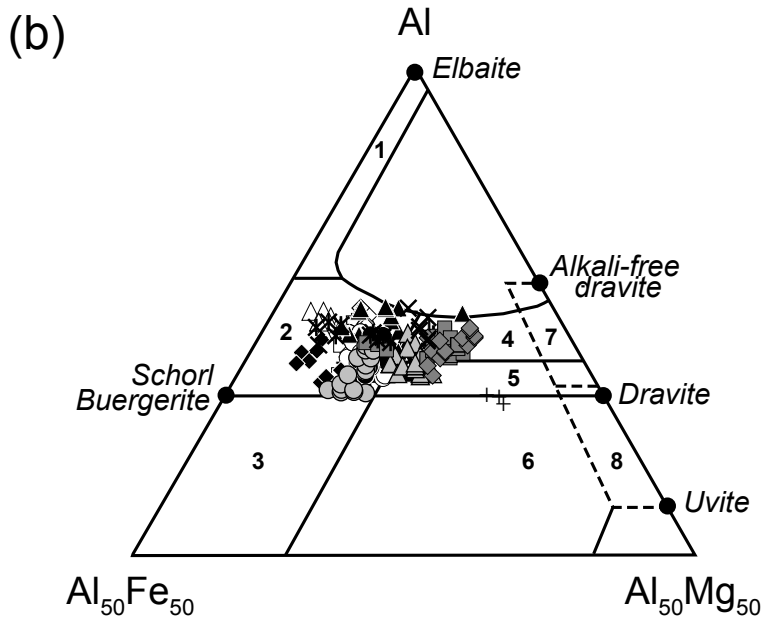

Mineralized samples	Barren samples
SS-1A-456 - wall rock	RO5-03-419 - wall rock NW-8030-1 - wall rock
GH-BB-19 - breccia GH-BB-23 - breccia JS-06-32B - breccia	AB-1-Beliel - breccia CoNiCu-tg - breccia BB-DC-4 - breccia
GH-BB-20 - stratabound ore zone SP-79-803 - stratabound ore zone	
	SA-1-3 - megacrystic granite SA-1-4 - megacrystic granite
	R97-15-221 - vein in wall rock 67SB160A - vein in granite

Trumbull et al. - Figure 3

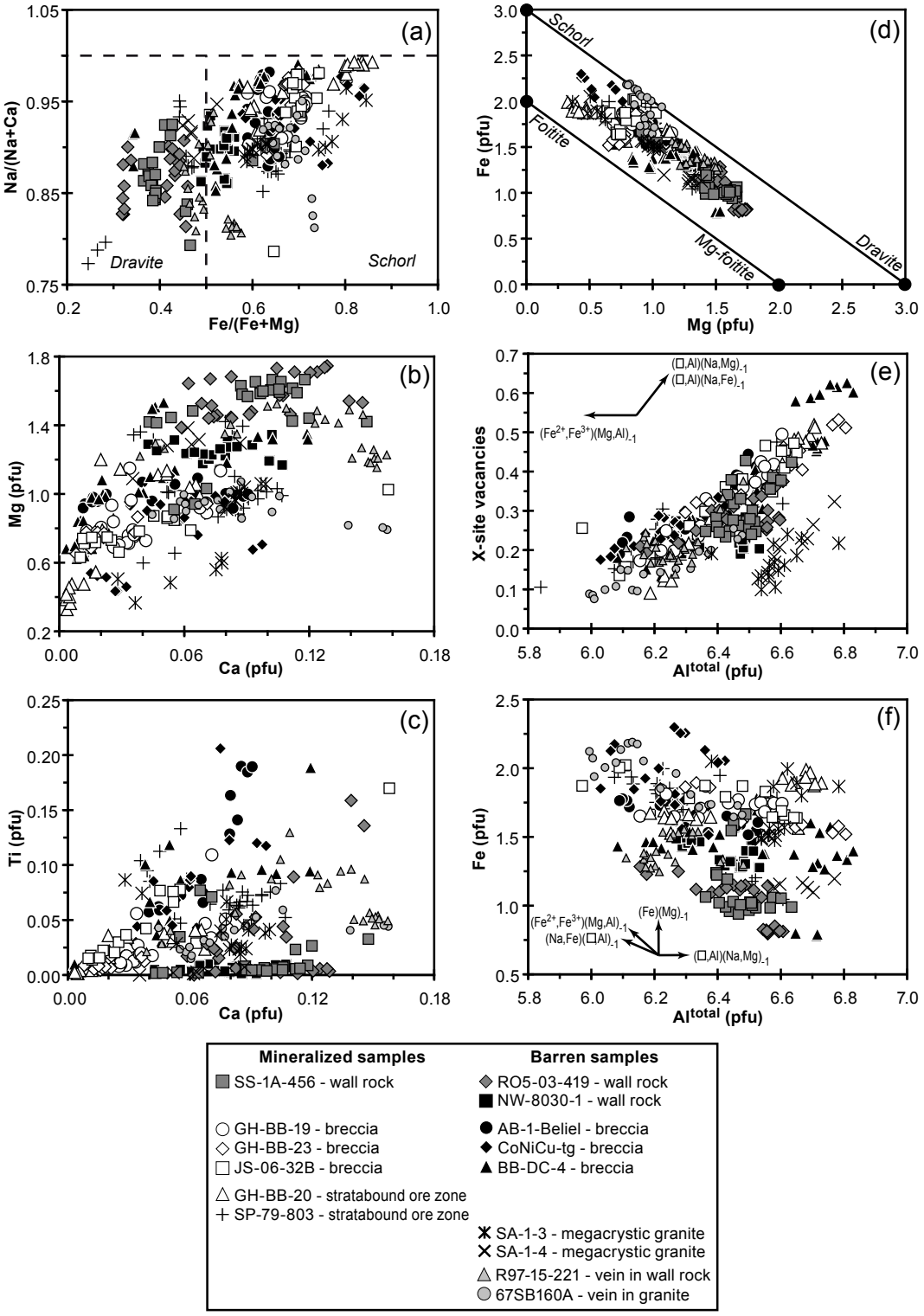

Trumbull et al. - Figure 4

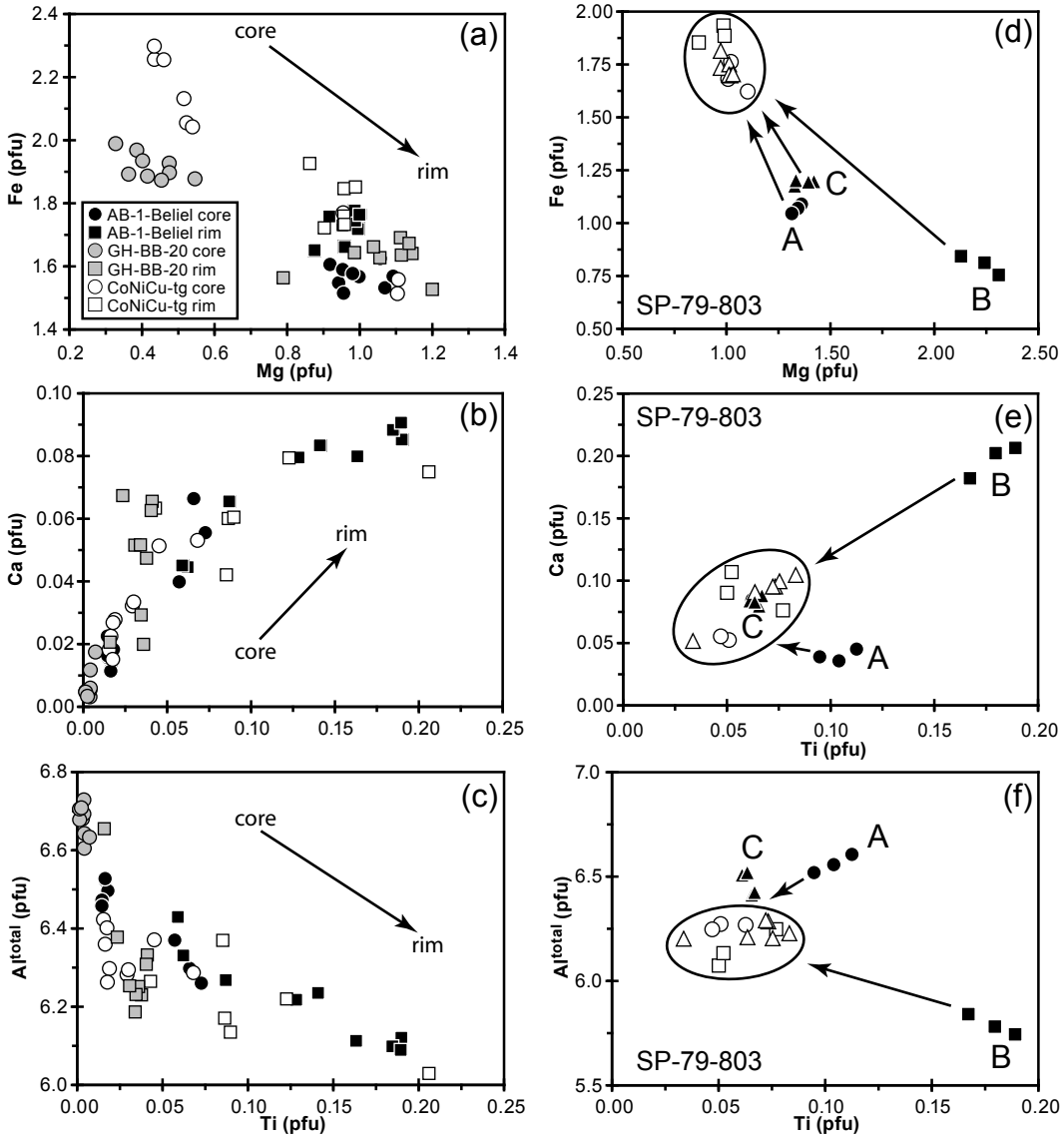

Trumbull et al. - Figure 5

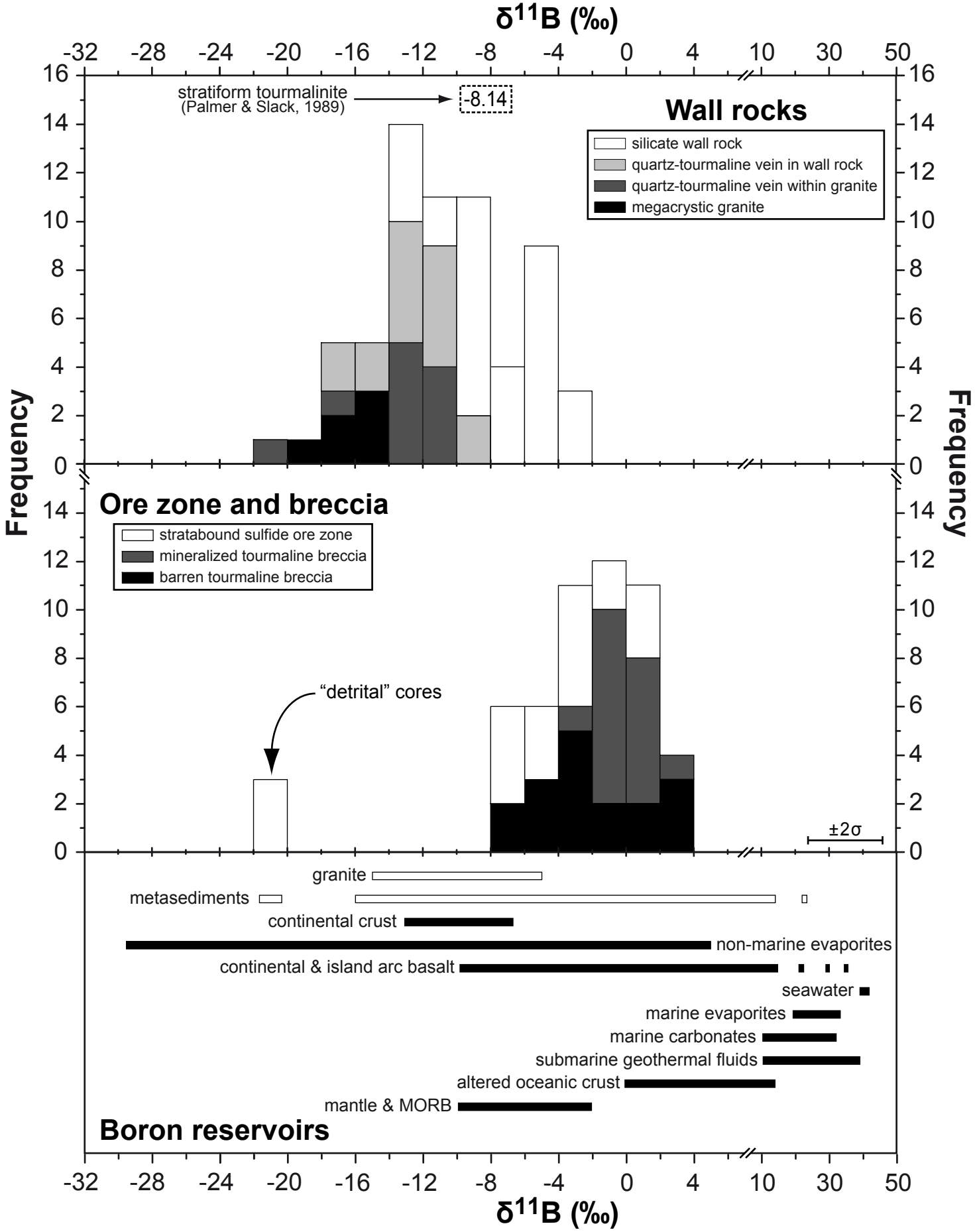

Trumbull et al. - Figure 6

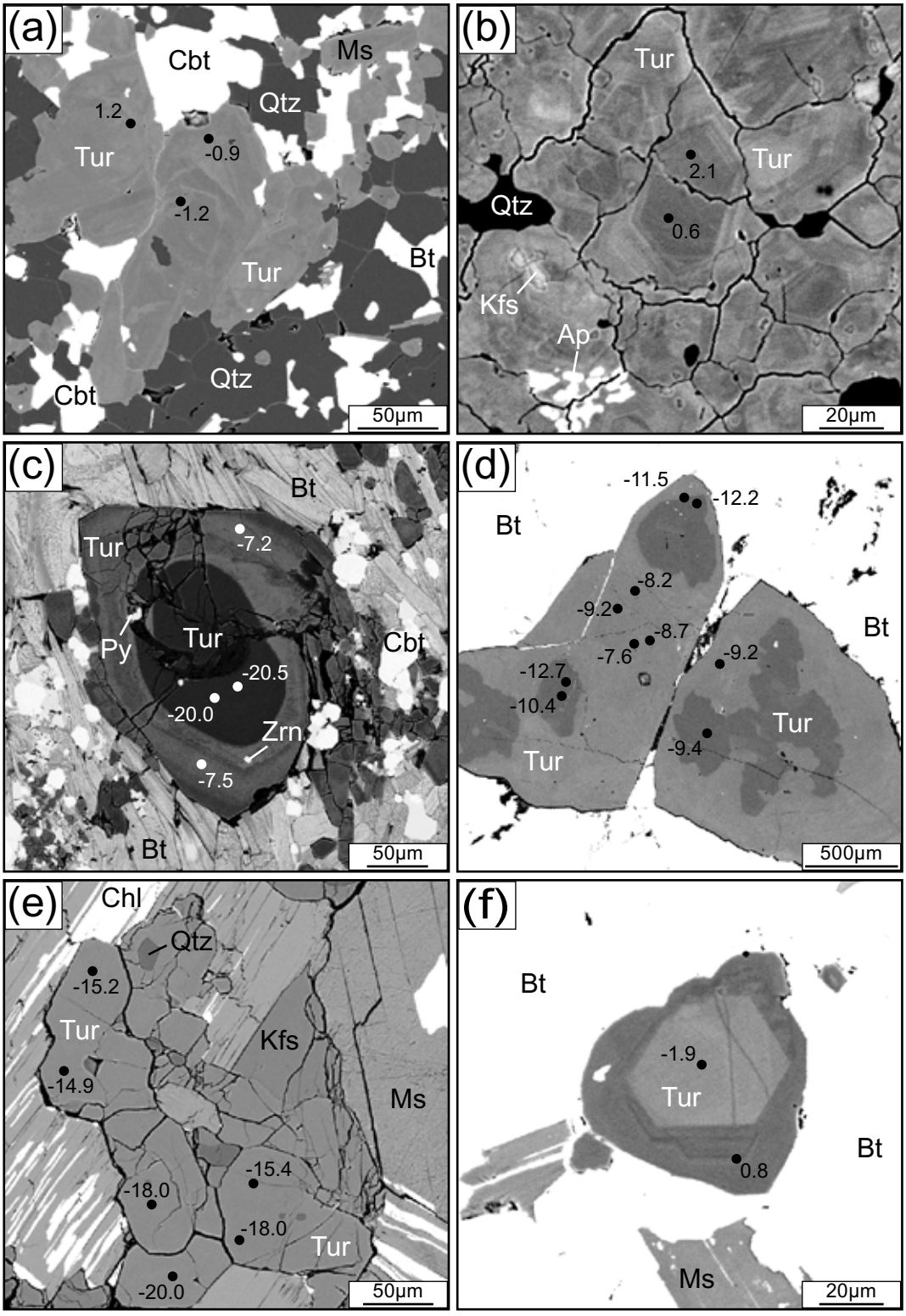

Trumbull et al. - Figure 7

Table 1 Selected electron-microprobe compositions of tourmaline from different lithotypes in the Blackbird district

Sample	GH-BB-20		SS-1A-456		JS-06-32B		AB-1-Beliel		R97-15-221		67SB160A		SA-1-4	
Lithotype	stratabound ore		qtz-chl-tur wall rock		mineralized breccia		barren breccia		qtz-tur vein in wall rock		qtz-tur vein in granite		megacrystic granite	
Position	core	rim	core	rim	core	rim	core	rim	core	rim	interior	interior	interior	-interior
SiO_2 (wt. %)	36.4	36.2	36.7	37.1	36.3	35.8	36.4	36.0	36.5	36.4	36.0	35.2	36.6	36.5
TiO_2	0.03	0.33	0.19	0.07	0.12	1.36	0.13	1.52	0.71	0.77	0.17	0.36	0.05	d.l.
Al_2O_3	34.6	32.7	33.9	33.9	33.7	30.4	33.8	31.3	32.1	32.0	33.6	31.1	34.6	35.1
MgO	1.48	4.32	5.93	7.02	2.57	4.13	3.86	4.02	6.02	5.80	3.92	3.46	5.46	5.30
MnO	d.l.	d.l.	d.l.	d.l.	d.l.	d.l.	d.l.	d.l.	d.l.	d.l.	d.l.	0.05	0.04	d.l.
FeO	13.7	11.9	8.85	7.98	13.3	13.4	11.3	12.4	9.8	10.1	12.1	15.4	8.5	8.1
Cr_2O_3	d.l.	0.03	d.l.	d.l.	d.l.	d.l.	d.l.	d.l.	d.l.	d.l.	d.l.	d.l.	d.l.	d.l.
CaO	0.03	0.37	0.65	0.69	0.06	0.89	0.07	0.48	0.84	0.77	0.33	0.49	0.39	0.30
Na_2O	1.62	2.24	1.75	2.05	1.63	1.80	1.81	1.93	1.95	2.10	2.20	2.34	2.29	2.15
K_2O	d.l.	0.04	d.l.	d.l.	d.l.	d.l.	d.l.	0.04	d.l.	0.06	d.l.	0.04	0.04	0.04
F	d.l.	d.l.	d.l.	d.l.	d.l.	d.l.	d.l.	d.l.	d.l.	d.l.	0.07	0.15	0.21	0.18
Cl	d.l.	d.l.	d.l.	d.l.	d.l.	d.l.	d.l.	d.l.	d.l.	d.l.	d.l.	d.l.	d.l.	d.l.
Sum	88.0	88.2	88.0	88.8	87.7	87.8	87.4	87.6	88.0	88.1	88.4	88.6	88.2	87.6
Si (atoms p.f.u.)	6.009	5.937	5.924	5.899	5.972	5.961	5.966	5.974	5.942	5.944	5.882	5.860	5.921	5.913
Al(T)	0.000	0.063	0.076	0.101	0.028	0.039	0.034	0.026	0.058	0.056	0.118	0.140	0.079	0.087
Al(Z)	6.000	6.000	6.000	6.000	6.000	5.932	6.000	6.000	6.000	6.000	6.000	5.953	6.000	6.000
Al(Y)	0.729	0.269	0.355	0.261	0.523	0.000	0.488	0.094	0.109	0.110	0.360	0.000	0.517	0.615
Ti	0.004	0.041	0.023	0.009	0.015	0.170	0.017	0.190	0.087	0.094	0.021	0.045	0.006	d.l.
Mg	0.363	1.056	1.424	1.666	0.631	1.025	0.942	0.995	1.462	1.412	0.956	0.858	1.316	1.281
Mn	d.l.	d.l.	d.l.	d.l.	d.l.	d.l.	d.l.	d.l.	d.l.	d.l.	d.l.	0.006	0.005	d.l.
Fe	1.893	1.628	1.193	1.063	1.829	1.871	1.548	1.718	1.338	1.382	1.660	2.135	1.155	1.098
Cr	d.l.	0.003	d.l.	d.l.	d.l.	d.l.	d.l.	d.l.	d.l.	d.l.	d.l.	d.l.	d.l.	d.l.
Ca	0.005	0.066	0.112	0.118	0.010	0.158	0.012	0.085	0.146	0.134	0.058	0.088	0.067	0.052
Na	0.518	0.712	0.547	0.633	0.521	0.581	0.575	0.621	0.616	0.665	0.698	0.755	0.718	0.676
K	d.l.	0.009	d.l.	d.l.	d.l.	0.005	d.l.	0.009	d.l.	0.013	d.l.	0.007	0.008	0.007
X-site vacancy	0.473	0.213	0.341	0.247	0.466	0.256	0.413	0.285	0.233	0.188	0.238	0.150	0.207	0.265

Mineral abbreviations: qtz- quartz, chl-chlorite, tur-tourmaline

Analyses by electron microprobe, total Fe reported as FeO, structural formula based on 15 cations in T, Z and Y sites (Henry & Dutrow, 1996). “d.l.” indicates below detection limit (0.02 – 0.04 wt.%, see text), all data are in electronic supplement ESM1

Table 2. Example of B-isotope results on reference tourmalines

Analysis date	$^{11}B/^{10}B$	1SD (‰)[a]	IMF[b]	$\delta^{11}B$ (‰)[c]
Schorl ($^{11}B/^{10}B$ = 3.993 and $\delta^{11}B$ = -12.5 ‰)				
12.08.2008	3.877	0.5	0.9709	-10.6
12.08.2008	3.881	0.5	0.9719	-9.6
12.08.2008	3.874	0.5	0.9702	-11.4
12.08.2008	3.872	0.8	0.9697	-11.9
Mean	3.876		0.9707	-10.9
Repeatability[d]	1.01			
Dravite ($^{11}B/^{10}B$ = 4.017 and $\delta^{11}B$ = -6.6 ‰)				
12.08.2008	3.893	0.4	0.9692	-6.5
12.08.2008	3.890	0.5	0.9684	-7.3
12.08.2008	3.893	0.8	0.9692	-6.5
12.08.2008	3.884	0.7	0.9669	-8.8
Mean	3.890		0.9684	-7.3
Repeatability[d]	1.09			
B4 ($^{11}B/^{10}B$ = 4.0078 and $\delta^{11}B$ = -8.9 ‰)				
12.08.2008	3.880	0.5	0.9681	-9.9
12.08.2008	3.880	0.6	0.9681	-9.9
12.08.2008	3.877	0.7	0.9674	-10.6
Mean	3.879		0.9679	-10.1
Repeatability[d]	0.45			

[a] Individual uncertainty for 100 cycles (standard deviation / mean) x 1000
[b] Instrumental mass fractionation ($^{11}B/^{10}B_{measured}$ / $^{11}B/^{10}B_{RM}$)
[c] Calculated with mean IMF of all reference tourmalines (0.9691), and with $^{11}B/^{10}B$ = 4.04362 for NIST SRM 951 (Cantanzaro et al.,1970)
[d] Repeatability from multiple analyses (standard deviation / mean) x 1000

Table 3. Summary of boron isotope composition of tourmaline from the Blackbird district

Sample	Lithotype and deposit	δ^{11}B range (‰)	SD	N analyses	Within-grain variations[a]
Mineralized samples					
SS-1A-456	mineralized qtz-chl-tur wall rock, Sunshine	-13.0 to -7.6	2.2	7	no
GH-BB-19	mineralized tur- breccia, Idaho	-3.1 to +2.5	2.7	4	no
GH-BB-23	mineralized tur- breccia, Haynes Stellite	-1.1 to +1.0	0.7	6	no
JS-06-32B	mineralized tur- breccia pipe, CoNiCu	-1.2 to +1.2	1.0	6	no
GH-BB-20	qtz-bio lens, stratabound ore, South Idaho	-6.9 to +1.6	2.9	8	5.3‰
SP-79-803	Stratabound sulfide zone, Brown Bear	-7.5 to -2.4[b]	1.7	9	2.9‰
Barren samples					
RO5-03-419	bio-gar-tur wall rock, Ram	-12.7 to -7.6	1.7	10	5.0‰
NW-8030-1	Stratiform tur-rich biotitite	-6.7 to -2.9	1.1	16	4.3‰
AB-1-Beliel	barren tur-breccia pipe, Beliel	-0.9 to +3.3	1.7	5	no
CoNiCu-tg	late, barren tur-qtz breccia in CoNiCu pipe	-7.2 to -2.1	2.2	5	no
BB-DC-4	barren brecciated quartzite with tur matrix	-4.6 to +0.5	2.0	7	4.1‰
SA-1-4	late magmatic/hydrothermal tur in granite	-20.0 to -14.9	2.0	6	5.0‰
R97-15-221	late qtz-tur vein in siltite, Ram	-17.0 to -9.2	2.2	16	7.8‰
67SB160A	late qtz-tur vein in granite margin	-12.8 to -10.2[c]	1.0	9	no

Mineral abbreviations: qzt- quartz, chl-chlorite, bio-biotite, tur-tourmaline

[a)] Range in single grains if >2‰, excluding outliers (see notes [b] and [c]); variations are patchy; no grains show significant zoning

[b)] Excluding 3 outlier core analyses (-20, -21.5, -21.1‰)

[c)] Excluding 2 outlier analyses (-17.4, -21.7‰)